# Low-Light Image and Video Enhancement: A Comprehensive Survey and Beyond

Shen Zheng, Yiling Ma\*, Jinqian Pan\*, Changjie Lu\*, Gaurav Gupta

Abstract—This paper presents a comprehensive survey of low-light image and video enhancement. We begin with the challenging mixed over-/under-exposed images, which are underperformed by existing methods. To this end, we propose two variants of the SICE dataset named SICE\_Grad and SICE\_Mix. Next, we introduce Night Wenzhou, a large-scale, high-resolution video dataset, to address the lack of low-light video datasets that discourages the use of low-light image enhancement (LLIE) methods in videos. Our Night Wenzhou dataset is challenging since it consists of fast-moving aerial scenes and streetscapes with varying illuminations and degradation. We then construct a hierarchical taxonomy, conduct extensive key technique analysis, and performs experimental comparisons for representative LLIE approaches using our proposed datasets and the current benchmark datasets. Finally, we identify emerging applications, address unresolved challenges, and propose future research topics for the LLIE community. Our datasets are available at https://github.com/ShenZheng2000/LLIE Survey.

Index Terms—Low-Light Image and Video Enhancement, Low-Level Vision, Deep Learning, Computational Photography.

## I. INTRODUCTION

Images are often captured under sub-optimal illumination conditions. Due to environmental factors (e.g., poor lightening, incorrect beam angle) or technical constraints (e.g., small ISO, short exposure) [1], these images often have deteriorated features, and low contrast (See Fig. 1), which not only deteriorate the low-level perceptual quality but also degrade the high-level vision tasks such as object detection [2], semantic segmentation [3], and depth estimation [4].

The aforesaid problem can be addressed in a logical manner from the camera side. The brightness of the images will undoubtedly improve with higher ISO and exposure. However, boosting ISO causes noise, whereas prolonged exposure produces motion blur [5], which makes the images look even worse. The other viable option is to enhance the visual appeal of low-light images using image editing tools like Photoshop or Lightroom. However, both tools demand artistic taste and take a long time on large datasets.

Unlike the camera and software approaches which demand manual efforts, low-light image enhancement (LLIE) aims to automatically improve the visibility of images taken in lowlight conditions. It is an active research field that is related to

Shen Zheng is with the School of Computer Science, Carnegie Mellon University, Pittsburgh, PA, USA (email: shenzhen@andrew.cmu.edu). Jinqian Pan is with the Center for Data Science, New York University, New York, NY, USA (email: jp6218@nyu.edu) . Yiling Ma, Changjie Lu, and Gaurav Gupta is with the School of Science and Technology, Wenzhou-Kean University, Wenzhou, Zhejiang, China (email: mayili@kean.edu, lucha@kean.edu, ggupta@kean.edu).



Fig. 1. Example images at challenging illumination conditions. First row: different exposures (E.). Second and third row: different lighting (L.) conditions. Bottom row: different degradation.

various system-level applications, such as visual surveillance [6], autonomous driving [7], unmanned aerial vehicle [8], photography [9], remote sensing [10], microscopic imaging [11], and underwater imaging [12].

In pre-deep learning eras, the only option for LLIE is the traditional approaches. Most traditional LLIE methods utilize Histogram Equalization [13], [14], [15], [16], [17], [18], [19], Retinex theory [20], [21], [22], [23], [24], [25], [26], Dehazing [27], [28], [29], [30], or Statistical methods [31], [32], [33], [18], [34]. While these traditional approaches have solid theoretical foundations, in practice they deliver unsatisfactory results.

The popularity of deep learning LLIE approaches can be attributed to their superior effectiveness, efficiency, and generalizability. Deep learning-based LLIE methods can be divided into the following categories: supervised learning [35], [36], [37], [38], [5], [39], [40], [41], [42], [43], [44], [45], [46], [47], [48], [49], [50], [51], [52], [53], [54], [55], [56], unsupervised learning [57], [58], semi-supervised learning [59] and zero-shot learning [60], [61], [62], [63], [64], [65] methods. In the past five years, there have been a handful of publications on deep learning-based LLIE (See Fig. 2 and Tab. I), and

<sup>\*</sup> Indicates equal contribution.



Fig. 2. Milestone for recent representative low-light image and video enhancement methods.

all learning algorithms have their strengths and limitations. For instance, unsupervised and zero-shot learning perform on unknown datasets, whereas supervised learning achieves state-of-the-art performance on benchmark datasets. It is crucial to carefully examine previous developments since they can offer a detailed knowledge, highlight present challenges, and suggest potential research directions for the LLIE community.

There are three recent surveys about LLIE. Wang et al. [66] reviews traditional learning-based LLIE methods. Liu et al. [67] propose a new LLIE dataset named VE-LOL, review LLIE methods, and introduce a joint image enhancement and face detection network named EDTNet. Li et al. [1] introduce a new LLIE dataset named LLIV-Phone, reviews deep learning-based LLIE methods, and design an online demo platform for LLIE methods.

The existing surveys have several limitations. Firstly, their proposed dataset has either overexposure *or* underexposure for single images. This assumption contradicts images from the real world, which frequently contain both overexposure *and* underexposure. Secondly, their proposed dataset contains few videos, and even these videos are filmed in fixed shooting positions. This oversimplification is also inconsistent with real-world videos that are often captured in motion. In addition, these studies emphasize low-level perceptual quality and high-level vision tasks while neglecting system-level application, which is essential when LLIE approaches are implemented in real-world products.

This paper makes the following contributions to the existing LLIE surveys:

- We present the most recent comprehensive survey on low-light image and video enhancement. In particular, we conducted an extensive qualitative and quantitative comparison with various full-reference and non-reference evaluation metrics and made a modularized discussion focusing on structures and strategies. Based on these analysis, we identity the emerging system-level applications, point out the open challenges and suggest directions for future works.
- We introduce two image datasets named SICE\_Grad and SICE\_Mix. They are the first datasets that include both overexposure and underexposure in single images. This preliminary effort highlights the LLIE community's unresolved mixed over- and underexposure challenge.

 We propose Night Wenzhou, a large-scale high-resolution video dataset. Night Wenzhou is captured during fast motions and contains diverse illuminations, various landscapes, and miscellaneous degradation. It will facilitate the application of LLIE methods to real-world challenges like autonomous driving and UAV.

The rest of the paper is organized as follows. Section II provides a systematic overview of existing LLIE methods. Section III introduces the benchmark datasets and the proposed datasets. Section IV makes empirical analysis and comparisons for representative LLIE methods. Section V identifies the system-level applications. Section VI discusses the open challenges and the corresponding future works. Section VII provides the concluding remarks.

#### II. METHODS REVIEW

# A. Selection Criteria

We select the LLIE methods according to the following rubrics. Firstly, we focus on LLIE methods in the recent 5 years (2018-2022) and lay emphasis on deep learning-based LLIE methods in the recent 2 years (2021-2022) because of their rapid development. Nevertheless, we also add three earlier works (2015-2017) to aid comparison. Secondly, we pick LLIE methods published in prestigious conferences (e.g., CVPR) and journals (e.g., TIP) with official codes to ensure credibility and authenticity. Thirdly, for the paper published in the same year, we prefer works with more citations and Github stars. Finally, we include LLIE methods that significantly surpass previous state-of-the-art benchmark LLIE datasets.

## B. Learning Strategies

Before 2017, traditional learning-based methods are the adhoc solution for LLIE. Since 2017, deep learning-based methods have started to dominate this field. Supervised learning (67.6 %) is so far the most popular strategy. From the year 2019, there are several methods using zero-shot learning (17.6 %), unsupervised learning (5.9 %), and semi-supervised (2.9 %). A hierarchical taxonomy for different learning strategies is shown in Fig. 3.

 $\label{table I} TABLE\ I$  Table Summary for recent representative low-light image and video enhancement methods.

Year	Name	Publications	Network Structures	Training Dataset	One-Sentence Summary
2015	PIE [68]	TIP	N/A	N/A	a probabilistic method for image enhancement based on
2016	LIME [69]	TIP	N/A	N/A	simultaneous illumination and reflectance estimation a LLIE method using illumination map estimation
2017	LLNet [35]	PR	U-Net	custom dataset	a deep autoencoder-based approach to adaptively brighten
					images with a high dynamic range
2018 2018	MBLLEN [36]	BMVC PRL	Multi-scale Others	custom dataset	a multi-branch fusion network for LLIE and LLVE a Retinex-based CNN for weakly illuminated image enhancement
	LightenNet [37]			custom dataset	a Retinex-based LLIE network using decomposition and
2018	Retinex-Net [38]	BMVC	Multi-scale	LOL	illumination adjustment
2018	SID [5]	CVPR	U-Net, Multi-scale	SID	a low-light image processing pipeline based on end-to-end training of a fully convolutional network
2019	DeepUPE [39]	CVPR	Others	custom dataset	a underexposed image enhancement network based on intermediate illumination with constraints and priors
2019	EEMEFN [40]	AAAI	U-Net	SID	a two-stage LLIE method named Edge-Enhanced Multi-Exposure Fusion Network
2019	ExCNet [60]	ACMMM	Others	custom dataset	a zero-shot CNN based on 'S-curve' estimation for back-lit image restoration
2019	KinD [41]	ACMMM	U-Net	LOL	a Retinex-based LLIE network using light adjustment and degradation removal
2020	Zero-DCE [61]	CVPR	Others	SICE	a zero-shot LLIE network based on high-order curves estimation and dynamic range adjustment
2020	DRBN [59]	CVPR	U-Net, Recursive	LOL	a semi-supervised deep recursive band network using band decomposition and recomposition for LLIE
2020	Xu et al. [42]	CVPR	U-Net, Multi-scale	custom dataset	a frequency-based decomposition and enhancement model for LLIE
2020	DLN [43]	TIP	Others	custom dataset	a Deep Lightening Network using Lightening Back-Projection blocks for LLIE
2020	DeepLPF [44]	CVPR	U-Net	MIT-Adobe-5K-DPE, MIT-Adobe FiveK,SID	a Deep Local Parametric Filters model using parameter regresion of spatially localized filters
2021 I	EnlightenGAN [57]	TIP	U-Net, Multi-scale	custom dataset	a unsupervised GAN using global-local discriminator, self-perceptual loss, and attention for LLIE
2021	KinD++ [45]	IJCV	U-Net	LOL	the extension of KinD
2021	Zero-DCE++ [62]	TPAMI	Others	SICE	the extension of Zero-DCE
2021	Zhang et al. [46]	CVPR	U-Net, Optical Flow	custom dataset	a method based on optical flow inference to enforce the temporal stability in LLVE with only static images.
2021	RUAS [63]	CVPR	NAS, Unfolding	MIT-Adobe FiveK,LOL	a Retinex-inspired unrolling model with Neural Architecture Search for LLIE
2021	UTVNet [47]	ICCV	U-Net, Unfolding	sRGB-SID	an adaptive unfolding total variation network based on noise level approximation and mapping for LLIE
2021	SDSD [48]	ICCV	Others	SDSD, SMID	a Retinex-based method using self-supervised noise reduction and illumination enhancement for LLVE
2021	RetinexDIP [64]	TCSVT	U-Net	N/A	a Retinex-based zero-shot method using generative decomposition and latent component estimation for LLIE
2022	SGZ [65]	WACV	U-Net, Recurrent	SICE	a zero-shot LLIE and LLVE network with pixel-wise light deficiency estimation and unsupervised semantic segmentation
2022	LLFlow [49]	AAAI	Normalizing Flow	LOL, VE-LOL	a normalizing flow-based LLIE model that consumes the low-light images/features as the condition
2022	SNR-Aware [50]	CVPR	Transformer	LOL, SID, SMID, SDSD	a signal-to-noise ratio aware transformer for LLIE
2022	SCI [58]	CVPR	Others	MIT-Adobe FiveK, LSRW, ACDC, DarkFace	a self-calibrated illumination learning framework for LLIE
2022	URetinex-Net [51]	CVPR	Unfolding	LOL	a Retinex-based deep unfolding network using initialization, unfolding optimization, and illimination adjustement for LLIE
2022	Dong et al. [52]	CVPR	U-Net	MCR, SID	a LLIE method fusing colored raw image and synthesized monochrome raw image from a De-Bayer-Filter simulator
2022	MAXIM [53]	CVPR	Transformer, Multi-scale	MIT-Adobe FiveK, LOL	a multi-axis multi-layer perceptron based transformer for low-level image processing tasks
2022	BIPNet [54]	CVPR	U-Net, Multi-scale	SID	a burst image restoration and enhancement approach based on pseudo-burst features and complementary information
2022	LCDPNet [55]	ECCV	U-Net, Multi-scale	custom dataset	a method based on local color distribution for over-/under-exposed region localization and enhancement
				LOL, MIT-Adobe FiveK,	an illumination adaptive transformer based on image

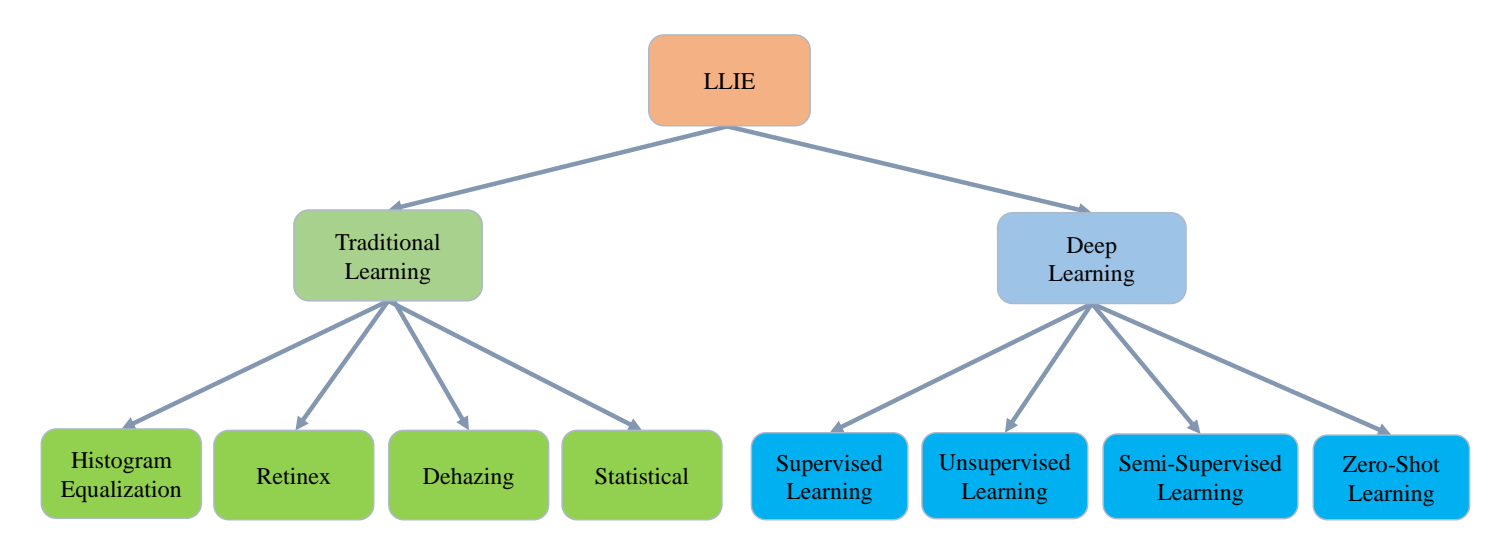


Fig. 3. A hierarchical taxonomy of learning strategies for low-light image and video enhancement methods.

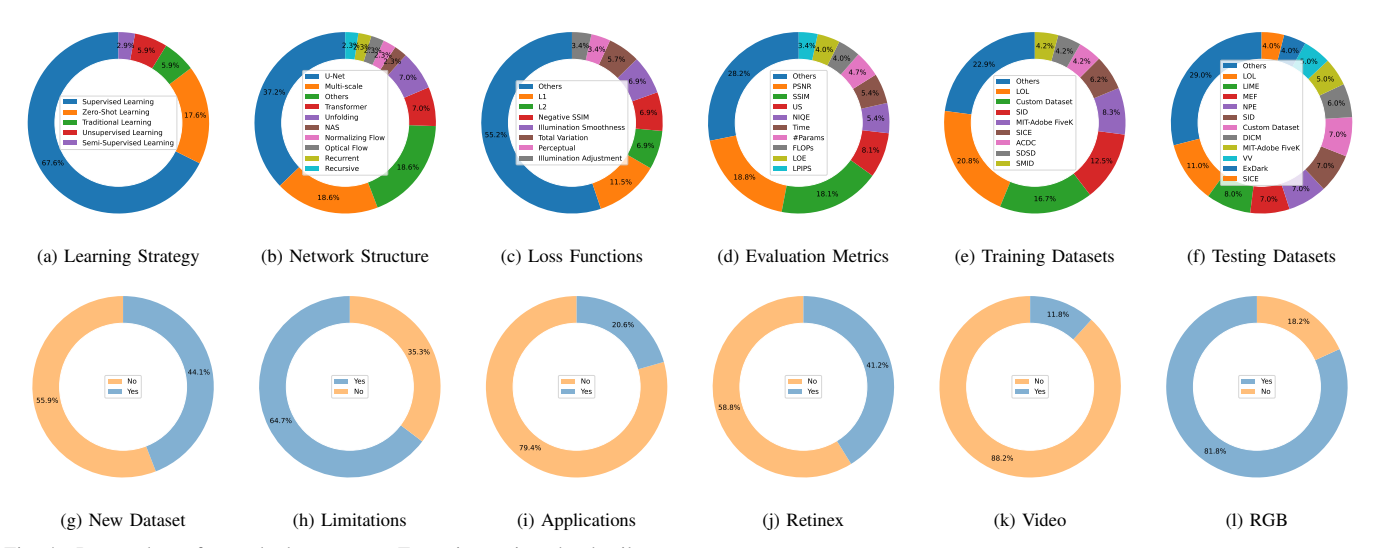


Fig. 4. Donut charts for methods summary. Zoom in to view the details.

1) Traditional Learning: Traditional Learning methods in LLIE refer to learning methods without neural networks. Instead, mainstream traditional learning methods in LLIE utilize Histogram Equalization, Retinex, Dehazing or Statistical techniques. A brief illustration is displayed in Fig. 5,

Histogram Equalization Histogram Equalization (HE)-based methods spread out the frequent intensity values of an image to improve its global contrast. In this way, the low-contrast region of an image gains higher contrast, and the visibility improves. The original HE-based method [13] consider global adjustment only, leading to poor local illumination and amplified degradation (e.g., noise, blur, and artifacts). The follow-up works attempt to address these issues using different priors and constraints. For example, Pizer et al. [14] perform HE on partitioned regions with local contrast constraints to suppress noise. Ibrahim et al. [70] utilize mean brightness preservation to prevent visual deterioration, whereas Arici et al. [15] additionally integrate contrast adjustment, noise robustness, and white/black stretching. The later works integrate gray-level

differences [16], depth information [17], weighting matrix [18], and visual importance [19] to guide low-light image enhancement towards better fine-grained details. In summary, the HE-based methods' performance gains are predominantly attributed to manually-designed constraints upon the vanilla histogram equalization.

Retinex Retinex-based methods are based on the Retinex theory of color vision [20], [21], which assumes that an image can be decomposed into a reflectance map and an illumination map. The enhanced image can be obtained by fusing the enhanced illumination map and the reflectance map. Lee et al. [22] is the pioneering work incorporating Retinex theory into image enhancement. After that, Wang et al. [23] utilizes lightness-order-error and bi-log transform to improve the naturalness and details during enhancement. Another work by Wang et al. [24] leverages Gibbs distributions as priors for the reflectance and illumination and gamma distributions as priors for the network parameters. Fu et al. [25] design a weighted variational model (instead of logarithmic transform)

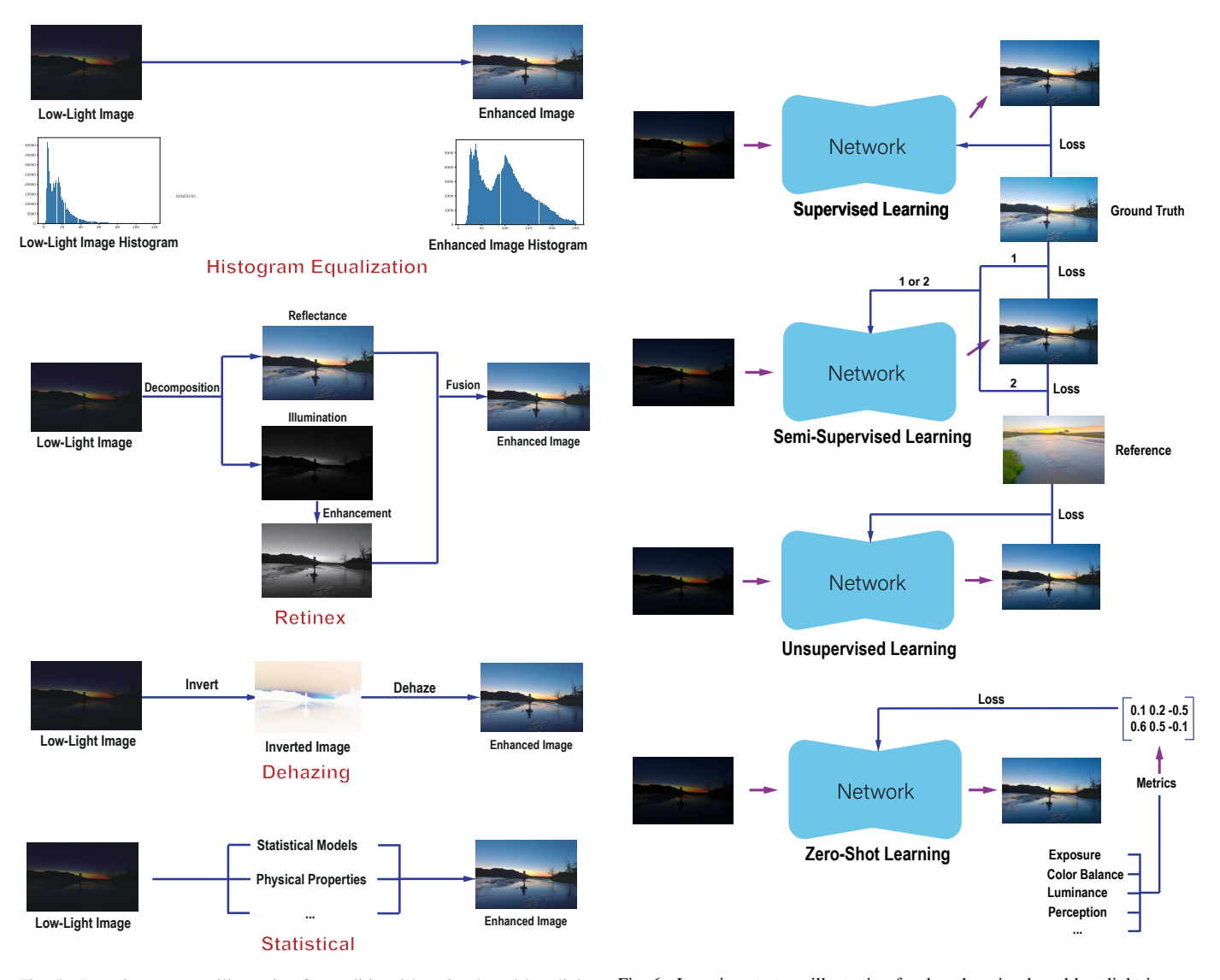


Fig. 5. Learning strategy illustration for traditional learning-based low-light image and video enhancement methods.

Fig. 6. Learning strategy illustration for deep learning-based low-light image and video enhancement methods.

for better prior modeling and edge preservation. Guo et al. [69] introduce a structure prior to refining the initial illumination map. Cai et al. [26] propose a shape prior for structural information preservation, a texture prior for reflection estimation, and an illumination prior for luminous modeling, respectively. In short, the Retinex-based models extensively rely on hand-crafted priors to achieve satisfactory image enhancement.

Dehazing Dehazing-based methods treat the inverted low-light images as haze images and then apply dehazing algorithms to enhance the image [27]. Instead of attending the whole image, Li et al. [28] decompose the images into base layers and details layers and use a dark channel prior [71]-guided dehazing process for image enhancement. Although less prevalent in LLIE, the dehazing-based methods have been widely used in underwater image enhancement. For example, Chiang et al. [29] leverage wavelength compensation, depth map estimation, and dehazing. The other work by Li et al. [30] builds an underwater image enhancement pipeline using the minimum information loss principle, histogram prior, and dehazing.

In brief, the dehazing largely depends on the insubstantial dehazing assumptions for performing enhancement.

Statistical Statistical methods involve statistical models and physical properties for image processing and enhancement. Compared with other traditional learning-based methods, statistical methods require a solid mathematical foundation and expert domain knowledge. The pioneering statistical method by Celik et al. [31] performs contrast adjustment using 2-D interpixel contextual information. Similar to HE-based approaches, the follow-up works to improve the previous research using additional constraints and assumptions. For example, Liang et al. [32] propose a variational model based on discrete total variation for local contrast adjustment. Yu et al. [33] utilize Gaussian surrounding function for light estimation, followed by light-scattering attenuation with information loss constraint for light refinement. Ying et al. [18] utilizes a weighting matrix for illumination estimation and a camera response model for best exposure ratio finding. Su et al. [34] exploit noise level function and a just noticeable difference model for noise suppression during image enhancement. In

essence, the Statistical methods are associated with computationally expensive optimization processes for performance improvements.

2) Deep Learning: In contrast to traditional learning methods, deep learning methods in LLIE include neural networks in their frameworks. The deep learning-based LLIE methods include four learning strategies, including supervised learning, unsupervised learning, semi-supervised learning, and zero-shot learning. A short illustration for these learning strategies is presented in Fig. 6.

Supervised Learning In LLIE, supervised learning refers to the learning strategy with paired images. For example, supervised learning may use one dataset with 1,000 low-exposure images and another with 1,000 normal-exposure images that are different in only illuminations. The pioneering work LLNet [35] utilizes a stacked sparse denoising autoencoder to exploit the multi-scale information for image enhancement. The subsequent work MBLLEN [36], for the first time, applies low-light image enhancement techniques to videos. Later, KinD [41] and KinD++ [45] combine model-based Retinex theory with data-driven image enhancement to cope with light adjustment and degradation removal. After that, Zhang et al. [46] exploit optical flow to promote stability in low-light video enhancement, whereas LLFlow leverages normalizing flow for illumination adjustment and noise suppression. The recent work IAT [56] proposes a lightweight illumination adaptive transformer for exposure correction and image enhancement. It is worth mentioning that the supervised learning method has achieved state-of-art-results on benchmark datasets.

Unsupervised Learning In LLIE, unsupervised learning refers to the learning strategy without paired images. For instance, unsupervised learning may use a dataset with low-exposure images and another with normal-exposure images that are different in more than illuminations. There are two unsupervised learning existing in LLIE literature. EnlightenGAN [57] is an unsupervised generative adversarial network (GAN) that regularizes unpaired learning using a multi-scale discriminator, a self-regularized perceptual loss, and the attention mechanism. SCI [58] introduces a self-calibrated illumination framework that utilizes a cascaded illumination learning process with weight sharing. Compared with supervised learning methods, unsupervised learning approaches avoids the tedious work of collecting paired training images.

Semi-supervised learning In LLIE, semi-supervised learning is a learning strategy with a small quantity of paired images and many unpaired images. An example will be a dataset with low-exposure images and another with normal-exposure images where most images are different in more than illuminations, and few images are different in only illuminations. To our knowledge, semi-supervised learning has been used by only one representative LLIE method named DRBN [59], which is based upon a recursive neural network with band decomposition and recomposition. Compared with supervised and unsupervised learning techniques, the potential of semi-supervised learning remains to be excavated.

**Zero-shot learning** In LLIE, zero-shot learning is a learning strategy that requires neither paired data nor unpaired training datasets. Instead, zero-shot learning learns image enhancement

at test time using data-free loss functions such as exposure loss or color loss. For example, ExCNet [60] introduces a zero-shot CNN based on estimating the "S-curve" that best fits the exposure of the back-lit images. Zero-DCE [61] and Zero-DCE++ [62] utilize zero-reference deep curve estimation and dynamic range adjustment. RUAS [63] develops a Retinex-inspired unrolling model with Neural Architecture Search (NAS). RetinexDIP [64] proposes a Retinex-based zero-shot method using generative decomposition and latent component estimation. SGZ [65] leverages pixel-wise light deficiency estimation and unsupervised semantic segmentation. Thanks to the zero-reference loss functions, zero-shot learning methods have outstanding generalization ability, require few parameters, and have fast inference speed.

**Discussion** The aforementioned traditional and deep learning strategies for LLIE have the following limitations.

- Traditional Learning methods' performances lag behind deep learning methods, even with their handcrafted priors and intricate optimization steps, which result in poor inference latency.
- Supervised Learning methods rely heavily on the paired training dataset, but none of the approaches for obtaining such a dataset is feasible. Specifically, it is difficult to capture image pairs that are only different in illuminations; it is hard to synthesize images that fit the complex real-world scenes; it is expensive and time-consuming to retouch large-scale low-light images.
- Unsupervised Learning methods' dependencies on the unpaired training dataset induces data bias. Because of data bias, unsupervised learning methods like EnlightenGAN (EGAN) [57] and SCI [58] generalize poorly to testing datasets with significant domain gaps.
- Semi-supervised learning methods inherit the limitations
  of both supervised and unsupervised learning methods
  without fully utilizing their strengths. That's why semisupervised learning has been used by only one representative LLIE method DRBN [59].
- Zero-shot learning methods require elaborate designs for the data-free loss functions. Still, they cannot cover all the necessary properties of real-world low-light images. Besides, their performances lag behind supervised learning methods like LLFlow [49] on benchmark datasets.

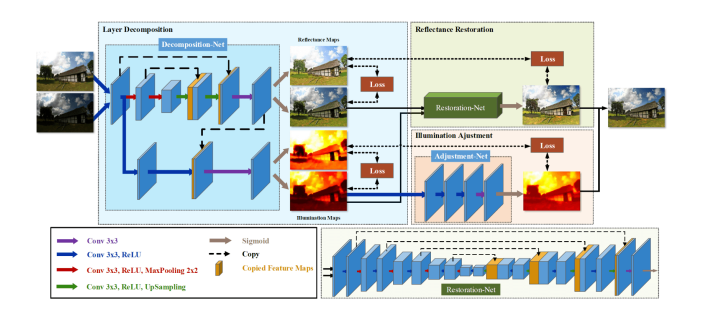


Fig. 7. Model Architecture of KinD [41], an U-Net-based LLIE method.

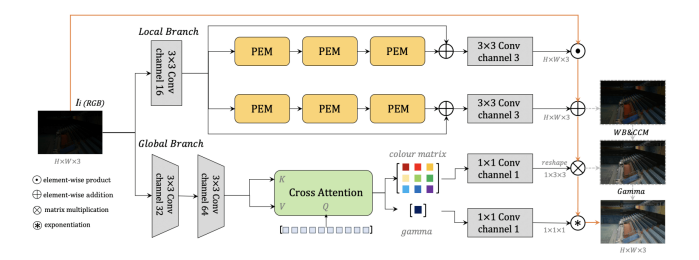


Fig. 8. Model Architecture of IAT [56], a Transformer-based LLIE method.

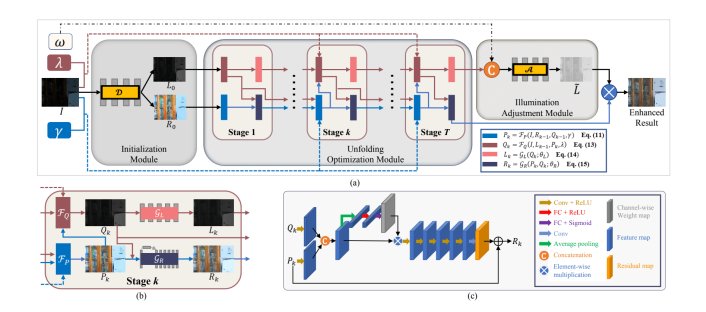


Fig. 9. Model Architecture of URetinex-Net [51], an unfolding-based LLIE method.

#### C. Network Structures

Many LLIE methods utilize a U-Net-like (37.2 %) structure or multi-scale information (18.6 %). Some methods use transformers (7.0 %) or unfolding networks (7.0 %). A few methods (2.3 % for each) use Neural Architecture Search (NAS), Normalizing Flow, Optical Flow, Recurrent Network, or Recursive Network.

**U-Net and multi-scale** U-Net-like [72] structure is the most popular in LLIE since it preserves high-resolution rich detail features and low-resolution rich semantic features, which are both essential for LLIE. Similarly, other structures that use multi-scale information are also welcomed in LLIE. Fig. 7 shows an example for U-Net-based method.

**Transformers** Recently, the transformers-based [73] method has surged in computer vision, especially high-level vision tasks, due to its ability to track long-range dependencies and capture global information in an image. Fig. 8 displays an example for transformer-based method.

**Unfolding and NAS** The unfolding network (a.k.a. unrolling network) [74] has been used by several methods because it combines the wisdom of model-based and data-based approaches. NAS [75] is the automating design of a neural network that generates the optimal result with a given dataset. Fig. 9 and 10 present examples for unfolding-based and NAS-based methods, respectively.

Normalizing and Optical Flow The normalizing flow-based [76] method transforms a simple probability distribution into a complex distribution with a sequence of invertible mappings, whereas optical flow-based [77] methods estimate the pixel-level motions of adjacent video frames. Fig. 11 and 12 are examples for normalizing flow-based and optical flow-based methods, respectively.

**Recurrent and Recursive** Recurrent network [78] is a type of neural network that repeatedly process the input in chain

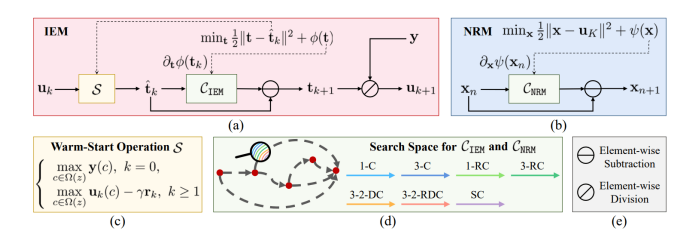


Fig. 10. Model Architecture of RUAS [63], a NAS-based LLIE method.

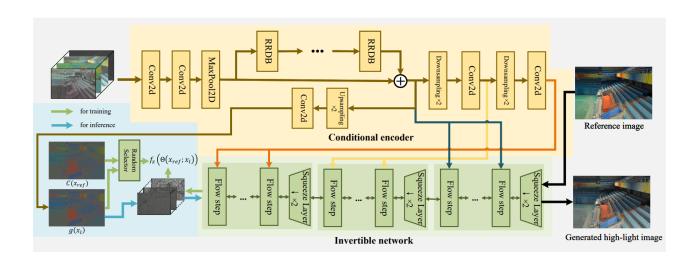


Fig. 11. Model Architecture of LLFlow [49], a normalizing flow-based LLIE method.

structures, whereas recursive network [79] is a variant of the recurrent network that processes the input in hierarchical structures. Fig. 13 and 14 shows examples for recurrent and recursive methods, respectively.

**Discussion** The aforementioned network structures for LLIE have the following limitations.

- Transformers is currently unpopular in low-level vision tasks like LLIE. Perhaps this is due to their impotence to integrate local and non-local attention and inefficiency at processing high-resolution images.
- The unfolding strategy requires elaborate network design, whereas NAS requires expensive parameter learning.
- The normalizing flow and optical flow-based methods have poor computational efficiency.
- The recurrent network have the vanishing gradient problem at large-scale data [80], whereas the recursive network relies on the inductive bias of hierarchical distribution, which is unrealistic.

# D. Loss Functions

The choice of loss functions is highly diverse among LLIE methods. 55.2 % of the LLIE methods use non-mainstream loss functions. Among mainstream loss functions,  $L_1$  (11.5 %) is the most popular, whereas  $L_2$  (6.9 %), Negative SSIM (6.9 %), and Illumination Smoothness (6.9 %) are also popular. A small quantity of methods use Total Variation (5.7 %), Perceptual (3.4 %), or Illumination Adjustment (3.4 %).

Full-Reference loss  $L_1$  loss,  $L_2$  loss, Negative SSIM loss, Perceptual loss [81] and Illumination adjustment loss [41] are full-reference loss functions (i.e., loss requiring paired images).  $L_1$  loss targets the absolute difference between image pairs, whereas  $L_2$  loss targets the squared difference. Therefore,  $L_2$  loss is rigid for large errors but tolerant for small errors, whereas  $L_1$  loss does the opposite. Like other low-level vision tasks [82],  $L_1$  loss in LLIE is more popular than  $L_2$  loss.

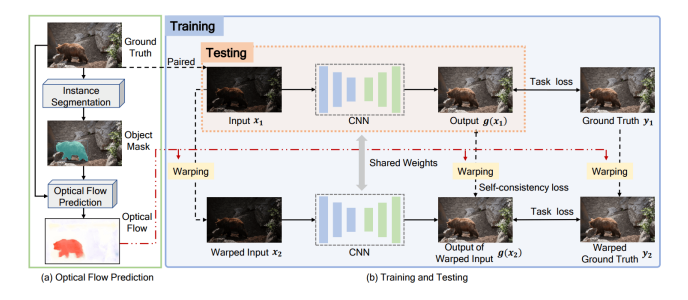


Fig. 12. Model Architecture of Zhang et al. [46], an optical flow-based LLVE method.

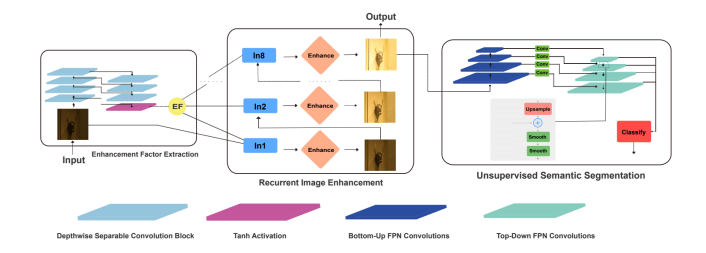


Fig. 13. Model Architecture of SGZ [65], a recurrent LLIE & LLVE method.

Negative SSIM loss is based upon the negative SSIM score. Essentially, it reflects the difference of image pairs in terms of luminance, contrast, and structure. However, Negative SSIM loss is uncommon in LLIE. That is different from other low-level vision tasks like image deraining, where it gains great popularity [83], [84], [85]. Perceptual loss is the  $L_2$  difference of image pairs based on their features extracted from a pretrained convolutional neural network (e.g., VGG-16 [86]). It is popular in low-level vision tasks like style transfer [81], [87] but is less explored in LLIE. Illumination adjustment loss is the  $L_2$  difference for illumination and illumination gradients between image pairs. Due to its task-specific nature, it has only been applied in LLIE algorithms [41], [45], [51].

Non-Reference loss Total Variation (TV) loss [88] and illumination smoothness loss [41] are non-reference loss functions (i.e., losses that do not require paired images). TV loss measures the sum of the difference between adjacent pixels in vertical and horizontal directions for an image. Therefore, TV loss suppresses irregular patterns like noise and blur and promotes smoothness in the image. Illumination smoothness loss is similar to TV loss since it is written as the  $L_1$  norm of illumination divided by the maximum variation. Despite their success at other low-level vision tasks like denoising [89] and deblurring [90], the variation-based methods have been less explored in LLIE.

## E. Evaluation Metrics

Many LLIE methods choose PSNR (18.8 %) or SSIM (18.1 %) as the evaluation metrics. Apart from PSNR and SSIM, the User Study (US) (8.1 %) is a popular method. Several methods use NIQE (5.4 %), Inference Time (5.4 %), #Params (4.7 %), FLOPs (4.0 %), LOE (4.0 %), or LPIPS (3.4 %) as the evaluation metrics.

Full-Reference Metrics Peak Signal-to-Noise Ratio (PSNR), Structure Similarity Index (SSIM), and Learned Perceptual

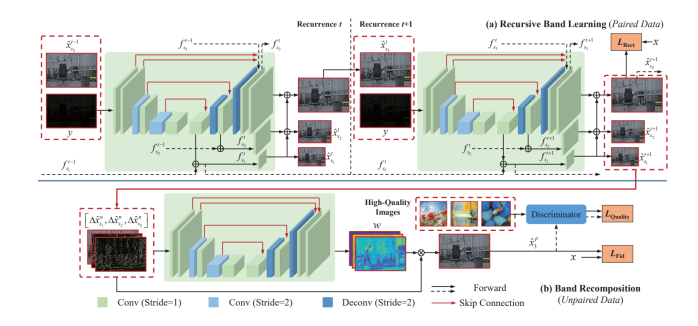


Fig. 14. Model Architecture of DRBN [59], a recursive LLIE method.

Image Patch Similarity (LPIPS) [91] are full-reference image quality evaluation metrics. PSNR measures the pixel-level similarity between image pairs, whereas SSIM measures the similarity according to luminance, contrast, and structure. LPIPS measures the patch-level difference between two images using a pretrained neural network. Higher PSNR and SSIM and lower LPIPS indicate better visual quality.

**Non-Reference Metrics** Natural Image Quality Evaluator (NIQE) [92] and Lightness order Error (LOE) [23] are non-reference image quality evaluation metrics. Specifically, NIQE is based on the naturalness score for an image using a model trained with natural scenes, whereas LOE indicate the lightness-order errors for that image. A lower NIQE and LOE indicate better visual quality.

**Subjective Metrics** User study is the only subjective metric used for representative LLIE methods. Typically, the user study score is the mean opinion score from a group of participants. A high user study score means better perceptual quality from human perspectives.

**Efficiency Metrics** Efficiency metrics include inference time, Numbers of Parameters (#Params), and Floating Point Operations (FLOPs). A shorter inference time and a smaller #Params and FLOPs indicates better efficiency.

## F. Training and Testing Data

Popular benchmark training data for LLIE include LOL (20.8 %), SID (12.5 %), and MIT-Adobe FiveK (8,3 %). Alternative choices include SICE (6.2 %), ACDC (4.2 %), SDSD (4.2 %), and SMID (4.2 %). Meanwhile, many utilize their custom dataset (16.7 %). Popular benchmark testing data for LLIE include LOL (11.0 %) and LIME (8.0 %). Some utilize MEF (7.0 %), NPE (7.0 %), and SID (7.0 %), while others use DICM (6.0 %), MIT-Adobe FiveK (5.0 %), VV (5.0 %), ExDark (4.0 %), or SICE (4.0 %). Similar to the case in training data, many methods utilize their custom dataset (7.0 %) for testing. A detailed discussion for training and testing dataset is given in Sec IV.

## G. Others

**New Dataset** The number of LLIE methods that introduce new datasets (55.9 %) surpasses the number of LLIE methods that only use existing datasets (44.1 %). This reflects the importance of data for LLIE.

TABLE II

TABLE SUMMARY FOR EXISTING BENCHMARK DATASET AND THE PROPOSED SICE\_GRAD AND SICE\_MIX. 'TRAINS' MEANS INCLUDING TRAINING DATASET. 'PAIRED' MEANS INCLUDING PAIRED IMAGES. 'TASK' MEANS QUALIFIED FOR HIGH-LEVEL VISION TASKS. THE ABBREVIATION 'Y', 'N', 'B' MEANS 'YES', 'NO', 'BOTH', RESPECTIVELY.

Dataset	Number	Resolutions	Type	Train	Paired	Task
NPE [23]	8	Various	Real	N	N	N
LIME [69]	10	Various	Real	N	N	N
MEF [93]	17	Various	Real	N	N	N
DICM [16]	64	Various	Real	N	N	N
VV	24	Various	Real	N	N	N
LOL [38]	500	$400 \times 600$	Real	Y	Y	N
VE-LOL [67]	13,440	Various	Both	В	Y	Y
ACDC [94]	4,006	$1080 \times 1920$	Real	Y	N	Y
DCS [65]	150	$1024 \times 2048$	Syn	N	Y	Y
DarkFace [95]	6,000	$720 \times 1080$	Real	Y	N	Y
ExDark [2]	7,363	Various	Real	Y	N	Y
MIT [96]	5,000	Various	Both	Y	Y	N
MCR [52]	3,944	$1024 \times 1280$	Both	Y	Y	N
LSRW [97]	5,650	Various	Real	Y	Y	N
TYOL [98]	5,991	Various	Syn	Y	Y	N
SID [5]	5,094	Various	Real	Y	Y	N
SDSD [48]	37,500	$1080 \times 1920$	Real	Y	Y	N
SMID [99]	22,220	$3672 \times 5496$	Real	Y	Y	N
SICE [100]	4,800	Various	Both	Y	Y	N
SICE_Grad	589	600×900	Both	Y	Y	N
SICE_Mix	589	600×900	Both	Y	Y	N

**Limitations** Most LLIE methods (64.7 %) do not mention their limitations and future works. This makes it hard for future researchers to improve upon their work.

**Applications** Most LLIE methods (79.4 %) do not relate low-level image enhancement to high-level applications like detection or segmentation. Therefore, the practical values of these methods remain a question.

**Retinex** Lots of methods (41.2 %) that utilize Retinex theory for LLIE enhancement. However, most LLIE methods (58.8 %) do not utilize Retinex theory. Hence, the Retinex theory remains a popular but non-dominant choice for LLIE.

**Video** A majority of LLIE methods (88.2 %) do not consider Low-Light Video Enhancement (LLVE) tasks. Sadly, most real-world low-light visual data are stored in video format.

**RGB** A majority of LLIE methods (81.8 %) uses RGB data for training. This is great since RGB is much more popular than RAW for modern digital devices like laptops or smartphones.

## III. DATASETS

## A. Benchmark Datasets

NPE[23]/LIME[69]/MEF [93]/DICM[16] carries 8/10/17/64 real low-light images of various resolutions. They contain indoor items and decorations, outdoor buildings, streetscapes, and natural landscapes, and they are all for testing.

**VV**<sup>1</sup> contains 24 real multi-exposure images of various resolutions. It contains traveling photos with indoor and outdoor persons and natural landscapes for testing.

**LOL** [38] contains 500 pairs of real low-light images of 400  $\times$  600 resolutions. It only contains indoor items and divides into 485 training images and 15 testing images.

VE-LOL [67] contains 13,440 real and synthetic low-light images and image pairs of various resolutions. It has diversified scenes, such as natural landscapes, streetscapes, buildings, human faces, etc. The paired portion VE-LOL-L has 2,100 pairs for training and 400 pairs for testing, whereas the unpaired portion VE-LOL-H has 6,940 images for training and 4,000 for testing. Additionally, the VE-LOL-H portion contains detection labels for high-level object detection tasks. ACDC [94] contains 4,006 real low-light images of resolution  $1,080 \times 1,920$ . It includes autonomous driving scenes with adverse conditions (1,000 foggy, 1,000 snowy, 1,000 rainy, and 1,006 nighttime) and has 19 classes. In particular, the ACDC nighttime contains 400 training images, 106 validation images, and 500 test images. Besides, ACDC contains semantic segmentation labels which allow high-level semantic segmentation tasks.

DCS [65] contains 150 synthetic low-light images of resolution  $1,024 \times 2,048$ . Specifically, it is synthesized with gamma correction upon the original CityScape [101] dataset, and it contains urban scenes with fine segmentation labels (30 classes). Therefore, it permits high-level instance segmentation, semantic segmentation, and panoptic segmentation tasks. The Dark CityScape (DCS) dataset is intended for testing only. DarkFace [95] contains 10,000 real low-light images of resolution  $720 \times 1,080$ . It contains nighttime streetscapes with many human faces in each image. It consists of 6,000 training and validation images and 4,000 testing images. With object detection labels, it can be applied to high-level object detection tasks.

**ExDark** [2] contains 7,363 real low-light images of Various resolutions. It contains images with diversified indoor and outdoor scenes under 10 illumination conditions with 12 object classes. It is split into 4,800 training images and 2,563 testing images. It contains object detection labels and can be applied to high-level object detection tasks.

**SICE** [100] contains 4,800 real and synthetic multi-exposure images of various resolutions. It contains images with diversified indoor and outdoor scenes with different exposure levels. The train/val/test follows a 7:1:2 ratio. In particular, SICE contains both normal-exposed and ill-exposed images. Therefore, it can be used for supervised, unsupervised, and zero-shot learning.

SID [5] contains 5,094 real short-exposure images, each with a matched long-exposure reference image. The resolution is  $4,240 \times 2,832$  for Sony and  $6,000 \times 4,000$  for Fuji images. The train/val/test follows a 7:1:2 ratio. It contains indoor and outdoor images, where the illuminance of the outdoor scene is 0.2lux 5lux, and the illuminance of the indoor scene is 0.03lux 0.3lux.

**SDSD** [48] contains 37,500 real images of resolution 1,080 × 1,920. It is the first high-quality paired video dataset for dynamic scenarios, containing identical scenes and motion in high-resolution video pairs in both low- and normal-light conditions.

**SMID** [99] contains 22,220 real low-light images of resolution  $3672 \times 5496$ . The dataset was randomly divided into 3 groups: training (64 %), validation (12 %), and testing (24 %). Some scenarios include various lighting setups, including light

<sup>&</sup>lt;sup>1</sup>https://sites.google.com/site/vonikakis/datasets

sources with various color temperatures, levels of illumination, and placements.

MIT Adobe FiveK [96] contains 5,000 real and synthetic images in diverse light conditions in various resolutions, including the RAW images taken directly from the camera and the edited versions created by 5 professional photographers. The dataset is divided into 80 % for training and 20 % for testing.

MCR [52] contains 3,944 real and synthetic short-exposure and long-exposure images of  $1,024 \times 1,280$  resolutions with monochrome and color raw pairs. The dataset is divided into train and test sets with a 9:1 ratio. The image are collected in both indoor fixed positions, and indoor/outdoor sliding platforms conditions.

**LSRW** [97] contains 5,650 real low-light paired images of various resolutions with indoor and outdoor scenes. 5,600 paired images are selected for training and the remaining 50 pairs are for testing.

**TYOL** [98] contains 5,991 synthetic images and most images conform to VGA resolution. It splits into 2,562 training images, 1,680 test images, and 1,669 test targets. The subset of TYOL, TYO-L (Toyota Light) contains texture-mapped 3D models of 12 objects with a wide range of sizes.

**Discussion** The current benchmark datasets for LLIE have the following limitations.

- Many datasets use synthetic images to meet the paired image requirement for supervised learning methods. These image synthesis techniques often follow simple gamma correction or exposure adjustment, which does not fit the diverse illuminations in the real-world. Consequently, methods trained with these synthetic images generalize poorly to the real-world images.
- The existing datasets consider single images rather than both images and videos. That is because that high-quality low-light videos are hard to capture and that many methods cannot process high-resolution video frames in real-time. However, the real-world applications (e.g., visual surveillance, autonomous driving, and UAV) are heavily dependent on videos rather than single images. Hence, the lack of low-light video dataset greatly undermines the benefits of LLIE for these fields.
- The existing datasets either consider underexposure or overexposure only, or consider underexposure and overexposure in separate images in a dataset. There is no dataset that contains mixed under-/overexposure in single images. See the detailed discussions in Subsection III-C.

## B. New Image Dataset

We synthesize two new datasets, dubbed SICE\_Grad and SICE\_Mix, based on the SICE [100] dataset. To obtain these two datasets, we first reshape the original SICE dataset to a resolution of  $600 \times 900$ . After that, we obtain panels from images in SICE with the same background but different exposures. The next step is different for SICE\_Grad and SICE\_Mix. For SICE\_Grad, we arrange the panels from low exposure to high exposure. To make it more challenging, we randomly placed some normally exposed panels at the end

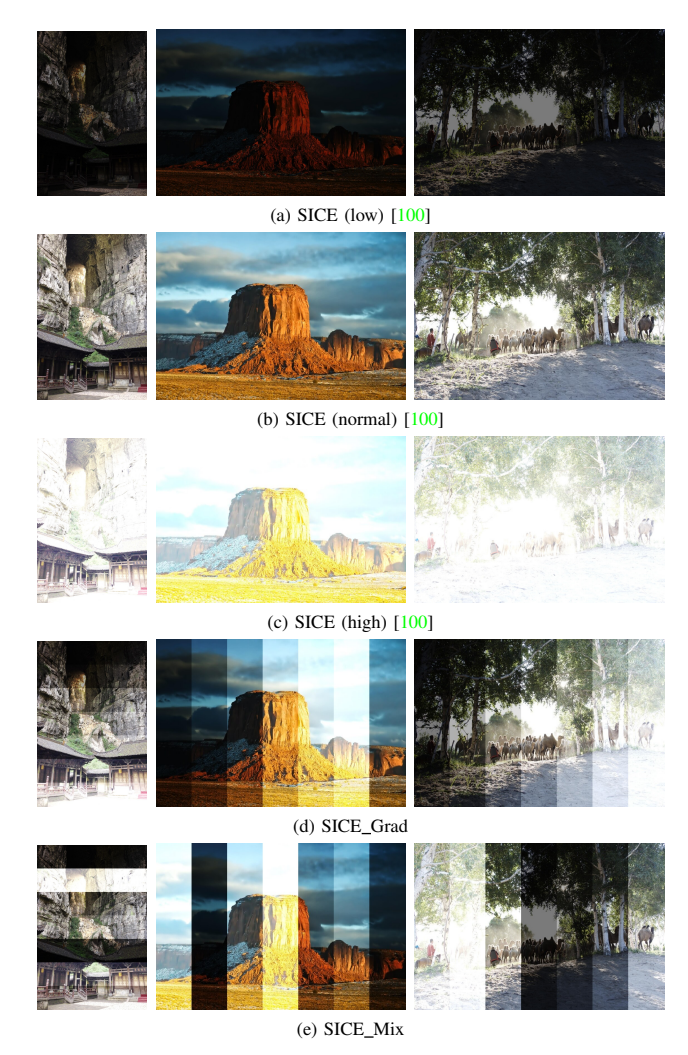


Fig. 15. Examples images for SICE (low-exposure, normal-exposure, high-exposure) and the proposed SICE\_Grad and SICE\_Mix.

instead of at the mid. For SICE\_Mix, we permute all panels at random. Example images for the original SICE and the proposal SICE\_Grad and SICE\_Mix are in Fig. 15. The table summary for SICE\_Grad and SICE\_Mix is shown in Tab. II.

Our SICE\_Grad and SICE\_Mix dataset has two significant advantages over existing datasets. Firstly, they are synthesized by permuting the panels of the SICE dataset. Therefore, we can use SICE\_Grad or SICE\_Mix paired with reshaped SICE dataset for training the supervised learning methods. On the other hand, we can also use SICE\_Grad and SICE\_Mix as testing datasets. Secondly, SICE\_Grad and SICE\_Mix contain extremely uneven exposure within a single image, often seen in real-world applications like UAVs.

#### C. Exposure Analysis

We conduct an exposure analysis to study the overexposure and underexposure for benchmark datasets with paired images. Specifically, we pick DCS [65], LOL [38], VE-LOL (Syn) [67], VE-LOL (Real) [67], and SICE [100] to compare with the proposed SICE\_Grad and SICE\_Mix.

The result of our exposure analysis is shown in Fig. 16. Specifically, we draw pixel-to-pixel scatter plots, where the

horizontal axis represents the pixel value for the input images, and the vertical axis represents the pixel value for the ground truth images. These plots have the following properties: 1) An individual curve describes an image pair. 2) a plot with only concave or convex curves means that the input dataset contains only under/over-exposed images. 3) a plot with both concave and convex curves means that the input dataset contains both over-exposed and under-exposed images. 4) a plot with individual curves that are both concave and convex means that there is mixed overexposure and underexposure in a single image.

We notice that DCS [65], LOL [38], VE-LOL (Syn) [67], and VE-LOL (Real) [67] contain under-exposed images only. SICE (low-exposure) has a majority of under-exposed images and a minority of over-exposed images, whereas SICE (high-exposure) has a majority of over-exposed images and a minority of under-exposed images. SICE\_Grad and SICE\_Mix are unique because they not only have over-exposed and under-exposed images across the whole dataset but also mixed overexposure and underexposure in single images. These characteristics make SICE\_Grad and SICE\_Mix particularly challenging for image enhancement. Our experiments in Section IV show that no representative LLIE method shows satisfactory result on SICE\_Grad or SICE\_Mix.

#### D. New Video Dataset

We collect a large-scale dataset named **Night Wenzhou** to comprehensively analyze the performance of existing methods in real-world low-light conditions. In particular, our dataset contains aerial videos captured with DJI Mini 2 and streetscapes captured with GoPro HERO7 Silver. All videos are taken nighttime in Wenzhou, Zhejiang, China, and have an FPS of 30. The table summary for Night Wenzhou is displayed in Tab. III. As we can see, Night Wenzhou contains videos of 2 hours and 3 minutes and has a size of 26.144 GB.

Our Night Wenzhou dataset is challenging since it contains large-scale high-resolution videos of diverse illumination conditions (e.g., extremely dark, underexposure, moonlight, uneven illumination, etc.). Besides, it contains various degradation (e.g., noise, blur, shadows, artifacts) commonly seen in real-world applications like autonomous driving. Our Night Wenzhou dataset can be used to train unsupervised and zero-shot learning methods and to test LLIE methods with any learning strategy. Sample images for our Night Wenzhou dataset are in Fig. 17.

## IV. EVALUATIONS

## A. Quantitative Comparisons

In this subsection, we leverage full-reference metrics including PSNR, SSIM, and LPIPS [102], and non-reference metrics including UNIQUE [103], BRISQUE [104], and SPAQ [105]. Note that some entries are 'N/A' due to the out-of-memory error during inference.

Tab. IV shows the quantitative comparison on LOL [38], DCS [65], VE-LOL [67], SICE\_Mix, and SICE\_Grad. We observe that LLFlow [49] demonstrates superior performance: it achieves the best PSNR, SSIM, and LPIPS on LOL [38]

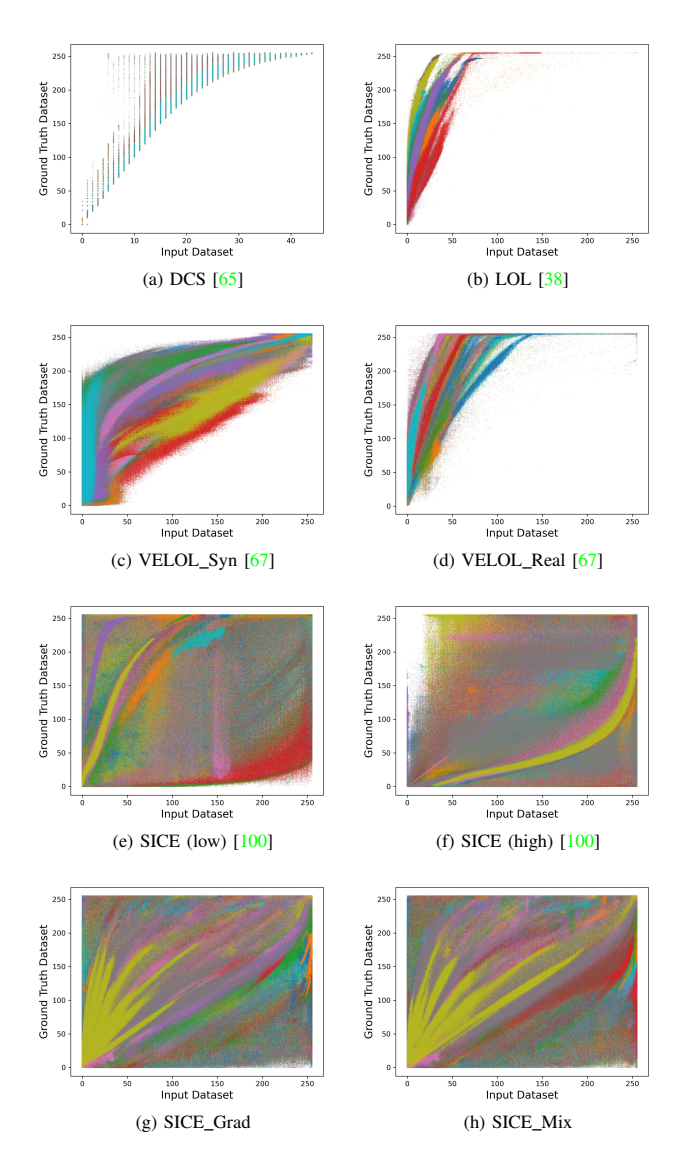


Fig. 16. Over-/underexposure analysis with different datasets that has paired images. For each subfigure, the horizontal axis refers to the input dataset, whereas the vertical axis refers to the ground truth dataset.

and VE-LOL (Real) [67], and the best PSNR and SSIM on DCS [65]. KinD++ [45] exhibits excellent performance with the best PSNR, SSIM, and LPIPS on VE-LOL (Syn) and SICE\_Mix, and the best PSNR and LPIPS on SICE\_Grad. Furthermore, Zero-DCE [61] has the best LPIPS on DCS [65], whereas KinD [41] has the best SSIM on SICE\_Grad. No other methods achieve the best score at any metrics.

Tab. V displays the quantitative comparison on NPE [23], LIME [69], MEF [93], DICM [16], and VV. We note that the competition for Tab. V is much more intense than Tab. IV. The only method with 4 best scores is Zero-DCE [61], whereas the only method with 3 best scores is KinD++ [45]. Besides, the methods with 2 best scores are RetinexNet [38] and SGZ [65]. Furthermore, the methods with only 1 best score include KinD [41], LLFlow [49], URetinexNet [51], and SCI [58]. RUAS [63] is the only method that does not perform the best at any metric.

Tab. VI presents the quantitative comparison on DarkFace

Device	Resolution	Duration (h:m:s)	Size (GB)
GoPro	1440 × 1920	0:09:08	1.871
GoPro	$1440 \times 1920$	0:13:04	2.675
GoPro	$1440 \times 1920$	0:17:41	3.727
GoPro	$1440 \times 1920$	0:17:40	3.727
GoPro	$1440 \times 1920$	0:17:43	3.727
GoPro	$1440 \times 1920$	0:11:15	2.316
GoPro	$1440 \times 1920$	0:05:14	1.029
GoPro	$1440 \times 1920$	0:17:57	3.727
GoPro	$1440 \times 1920$	0:02:25	0.526
GoPro Total		1:52:07	23.325
DJI	$1530 \times 2720$	0:01:47	0.500
DJI	$1530 \times 2720$	0:00:27	0.126
DJI	$1530 \times 2720$	0:00:42	0.198
DJI	$1530 \times 2720$	0:00:42	0.177
DJI	$1530 \times 2720$	0:00:27	0.127
DJI	$1530 \times 2720$	0:06:21	1.604
DJI	$1530 \times 2720$	0:00:27	0.087
DJI Total		0:10:53	2.819
Total		2:03:00	26.144

TABLE III
TABLE SUMMARY FOR NIGHT WENZHOU DATASET.

[95] and ExDark [2]. We notice that RUAS [63] earns the best UNIQUE and BRISQUE on DarkFace [95], whereas RetinexNet [38] scores the best SPAQ on DarkFace [95] and ExDark [2]. Additionally, LLFlow [49] obtains the best UNIQUE on ExDark [2].

The quantitative comparison of model efficiency is presented in Tab. VII. We choose ACDC [94] as the benchmark for efficiency comparison since it contains images of 2K resolution (i.e.,  $1080 \times 1920$ ), which is closer to real-world applications such as autonomous driving, UAV, and photography. It is shown that SGZ [65] obtains the best FLOPs and Inference Time, whereas SCI [58] gains the best #Params. Besides, it is worth mentioning Zero-DCE [61], RUAS [63], SGZ [65], and SCI [58] achieve real-time processing on a single GPU.

The quantitative comparison of semantic segmentation is shown in Tab. VIII. For both ACDC [94] and DCS [65], we feed the enhanced image into a semantic segmentation model named PSPNet [106] and calculate the mPA and mIoU score with the default thresholds. On ACDC [94], LLFlow [49] leads to the best mPA, whereas SCI [58] results in the best mIoU. On DCS [65], SGZ [65] contributes to the best mPA and mIoU.

The quantitative comparison of object detection is displayed in Tab. IX. In particular, we feed the enhanced image into a face detection model named DSFD [107] and calculate the IoU score with different IoU thresholds (0.5, 0.6, and 0.7). It is shown that LLFlow [49] yields the best IoU with all given thresholds.

## B. User Studies

Since there are few effective metrics to evaluate the visual quality of low-light video enhancement, we conducted a user study to assess the performances of different methods on the proposed Night Wenzhou dataset. Specifically, we ask 100 adult participants to watch the enhancement results of 7 models, including EGAN [57], KinD [41], KinD+ [45], MBLLEN [36], RetinexNet [38], SGZ [65], and Zero-DCE



Fig. 17. Video frames from our Night Wenzhou dataset.

[61]. They are asked to vote '1' to '5' for each method, where '1' indicates the worst performance, and '5' indicates the best.

We make a stacked bar graph in Fig. 18 to show the category-wise information for different methods. It can be seen that RetinexNet [38] has the most (37 %) of '1's; Zero-DCE [61] has the most (33 %) of '2's; EGAN [57] has the most (40 %) of '3's; MBLLEN has the most (45 %) of '4's; SGZ [65] has the most (39 %) of '5's. Therefore, RetinexNet [38] is voted to have the worst performance, whereas SGZ [65] is voted to have the best performance.

# C. Qualitative Comparisons

Fig. 19 presents the qualitative comparison on an image from the LOL [38] dataset. Our finding are as follows: 1) RUAS [63] produce over-exposed result 2) MBLLEN [36] over-smooth the image. 3) PIE [68], LIME [69], Zero-DCE [61], SGZ [65], and SCI [58] yield noise. 3) KinD [41], LLFlow [49], and URetinexNet [51] are close to GT.

Fig. 20 shows the qualitative comparison for an image from the VV dataset. Our finding are as follows: 1) RUAS [63] produces under-exposed trees. 2) RUAS [63], SCI [58], and URetinexNet [51] renders over-exposed skies. 3) LIME [69], Zero-DCE [61], and LLFlow [49] generates artifacts. 4) MBLLEN [36] oversmooths the image. 5) LLFlow [49] yield color distortion. 6) PIE [68], KinD [41], and SGZ [65] have a promising perceptual quality.

Fig. 21 and Fig. 22 display the qualitative comparison for an image from our SICE\_Grad dataset and the SICE\_Mix dataset, respectively. We find that no method yields faithful result on SICE\_Grad or SICE\_Mix. In particular, most methods successfully enhanced the under-exposed regions but made the over-exposed region even brighter. The lack of contrast from the homogeneous over-exposure makes it hard to distinguish any detail in these enhanced regions.

The qualitative comparison (w/ object detection) for an image from the DarkFace dataset [95] is shown in Fig. 23. In particular, the bounding box in the figure is annotated with the predicted class and probability. Our findings are as follows: 1) KinD [41], Zero-DCE [61], RUAS [63], SGZ [65], and SCI [58] produces under-exposure images, especially for the right

TABLE IV QUANTITATIVE COMPARISON ON LOL [38], DCS [65], VE-LOL (SYNTHETIC & REAL) [67], SICE\_MIX, AND SICE\_GRAD WITH PSNR $\uparrow$ , SSIM $\uparrow$ , AND LPIPS $\downarrow$ .

Methods	LOL [38]				\ \ \ \ \ \ \ \ \ \ \ \ \ \ \ \ \ \ \		VE-LOL (Real) [67]		_		SICE_Grad							
Methous	PSNR	SSIM	LPIPS	PSNR	SSIM	LPIPS	PSNR	SSIM	LPIPS	PSNR	SSIM	LPIPS	PSNR	SSIM	LPIPS	PSNR	SSIM	LPIPS
RetinexNet[38]	17.559	0.645	0.381	N/A	N/A	N/A	15.606	0.449	0.769	17.676	0.642	0.441	12.397	0.606	0.407	12.450	0.619	0.364
KinD[41]	15.867	0.637	0.341	13.145	0.720	0.304	16.259	0.591	0.432	20.588	0.818	0.143	12.986	0.656	0.346	13.144	0.668	0.302
Zero-DCE[61]	14.861	0.562	0.330	16.224	0.849	0.172	14.071	0.369	0.652	18.059	0.580	0.308	12.428	0.633	0.362	12.475	0.644	0.314
KinD++[45]	15.724	0.621	0.363	N/A	N/A	N/A	16.523	0.613	0.411	17.660	0.761	0.218	13.196	0.657	0.334	13.235	0.666	0.295
RUAS[63]	11.309	0.435	0.377	11.601	0.412	0.449	12.386	0.357	0.642	13.975	0.469	0.329	8.684	0.493	0.525	8.628	0.494	0.499
SGZ[65]	15.345	0.573	0.334	16.369	0.854	0.204	13.830	0.385	0.664	18.582	0.584	0.309	10.866	0.607	0.415	10.987	0.621	0.364
LLFlow[49]	19.341	0.839	0.142	20.385	0.897	0.240	15.440	0.476	0.517	24.152	0.895	0.098	12.737	0.617	0.388	12.737	0.617	0.388
URetinexNet[51]	17.278	0.688	0.302	16.009	0.755	0.369	15.273	0.466	0.591	21.093	0.858	0.103	10.903	0.600	0.402	10.894	0.610	0.356
SCI[58]	14.784	0.525	0.333	14.264	0.689	0.249	12.542	0.373	0.681	17.304	0.540	0.307	8.644	0.529	0.511	8.559	0.532	0.484

TABLE V QUANTITATIVE COMPARISON ON NPE [23], LIME [69], MEF [93], DICM [16], AND VV WITH UNIQUE (UNI $\uparrow$ ), BRISQUE (BRI $\downarrow$ ), AND SPAQ $\uparrow$ .

Methods		NPE [23	]	]	LIME [6	9]		MEF [93	3]	]	DICM [1	6]		VV	
Methous	UNI	UNI	SPAQ	UNI	UNI	SPAQ									
RetinexNet [38]	0.801	16.533	71.264	0.787	24.31	70.468	0.742	14.583	69.333	0.778	22.877	62.550	N/A	N/A	N/A
KinD [41]	0.792	20.239	70.444	0.766	39.783	67.180	0.747	32.019	63.266	0.776	33.092	59.946	0.814	29.439	61.453
Zero-DCE [61]	0.814	17.456	72.945	0.811	20.437	67.736	0.762	17.321	66.864	0.777	27.560	57.402	0.836	34.656	60.716
KinD++ [45]	0.801	19.507	71.742	0.748	19.954	73.414	0.732	27.781	67.831	0.774	27.573	62.744	N/A	N/A	N/A
RUAS [63]	0.706	47.852	61.598	0.783	27.589	62.076	0.713	23.677	60.701	0.710	38.747	47.781	0.770	38.370	47.443
SGZ [65]	0.783	14.615	72.367	0.789	20.046	67.735	0.755	14.463	66.134	0.777	25.646	55.934	0.824	31.402	58.789
LLFlow [49]	0.791	28.861	67.926	0.805	27.060	66.816	0.710	30.267	67.019	0.807	26.361	61.132	0.800	31.673	61.252
URetinexNet [51]	0.737	25.570	70.066	0.816	24.222	67.423	0.715	22.346	66.310	0.765	26.453	59.856	0.801	30.085	55.399
SCI	0.702	28.948	64.054	0.747	23.344	64.574	0.733	15.335	64.616	0.720	31.263	48.506	0.779	26.132	48.667

TABLE VI QUANTITATIVE COMPARISON ON DARKFACE [95] AND EXDARK [2] WITH UNI $\uparrow$ , BRI $\downarrow$ , AND SPAQ $\uparrow$ .

Methods	D	arkFace [	ExDark [2]			
Methous	UNI	BRI	SPAQ	UNI	SPAQ	
RetinexNet [38]	0.737	18.574	54.966	0.708	66.330	
KinD [41]	0.737	48.311	41.070	0.728	55.690	
Zero-DCE [61]	0.720	26.194	47.868	0.729	52.700	
KinD++ [45]	0.719	32.492	52.905	0.723	61.036	
RUAS [63]	0.740	13.770	42.329	0.712	47.785	
SGZ [65]	0.713	24.647	47.392	0.729	51.236	
LLFlow [49]	0.708	22.284	51.544	0.735	56.116	
URetinexNet [51]	0.739	15.148	51.290	0.722	57.291	
SCI [58]	0.719	19.511	46.046	0.709	50.618	

TABLE VII
EFFICIENCY COMPARISON ON ACDC [94] (RESOLUTION OF 1080 × 1920) WITH FLOPS,, #PARAMS,, AND INFERENCE TIME, USING A SINGLE NVIDIA GEFORCE RTX 3090 GPU. Blue INDICATES REAL-TIME CAPABILITY.

Methods	FLOPs	#Params	Time
RetinexNet [38]	N/A	0.5550	N/A
KinD [41]	1103.9117	8.1600	3.5288
Zero-DCE [61]	164.2291	0.0794	0.0281
KinD++ [45]	N/A	8.2750	N/A
RUAS [63]	6.7745	0.0034	0.0280
SGZ [65]	0.2135	0.0106	0.0026
LLFlow [49]	892.7097	1.7014	0.3926
URetinexNet [51]	1801.4110	0.3401	0.2934
SCI [58]	0.7465	0.0003	0.0058

half. Therefore, many objects in their enhanced image are not detected. 2) KinD [41] produces oversmoothed result. That is why the object detector is way off target in its enhanced image. 3) KinD++ [45], URetinexNet [51] and LLFlow [49] are good in terms of image enhancement. However, both KinD++ [45]

TABLE VIII

SEMANTIC SEGMENTATION RESULT COMPARISON ON ACDC [94] AND DCS [65] WITH MPA† (%) AND MIOU† (%).

ACDC	[94]		DCS [65]					
Methods	mPA	mIoU	Methods	mPA	mIoU			
KinD [41]	60.79	49.18	PIE [68]	68.89	61.97			
Zero-DCE [61]	59.00	49.51	RetinexNet [38]	66.76	57.96			
RUAS [63]	50.42	44.48	MBLLEN [36]	59.06	51.98			
SGZ [65]	61.65	49.50	KinD [41]	71.69	63.42			
LLFlow [49]	62.68	49.30	Zero-DCE [61]	74.20	64.36			
URetinexNet [51]	62.32	48.71	Zero-DCE++ [62]	74.43	65.51			
SCI [58]	57.52	49.66	SGZ [65]	74.50	65.87			

TABLE IX OBJECT DETECTION RESULT COMPARISON ON DARKFACE WITH DIFFERENT IOU THRESHOLDS. EACH NUMERICAL ENTRY IS A MAP  $\uparrow$  VALUE.

Learning	Methods	IoU@0.5	IoU@0.6	IoU@0.7
TL	LIME [69]	0.244	0.083	0.010
	LLNet [35]	0.228	0.063	0.006
	LightenNet [37]	0.270	0.085	0.011
SL	MBLLEN [36]	0.269	0.092	0.012
SL	KinD [41]	0.255	0.081	0.010
	KinD++ [45]	0.271	0.090	0.011
	URetinexNet [51]	0.283	0.101	0.015
	LLFlow [49]	0.290	0.103	0.016
UL	EGAN [57]	0.261	0.088	0.012
	ExCNet [60]	0.276	0.092	0.010
ZSL	Zero-DCE [61]	0.281	0.092	0.013
ZSL	Zero-DCE++ [62]	0.278	0.090	0.012
	SGZ [65]	0.279	0.092	0.012

and URetinexNet [51] yield artifacts. That's why LLFlow's [49] enhancement yields better object detection results.

The qualitative comparison (w/ semantic segmentation) for an image from the DCS dataset [65] is displayed in Fig. 24. Particularly, different colors are used to distinguish pixels from

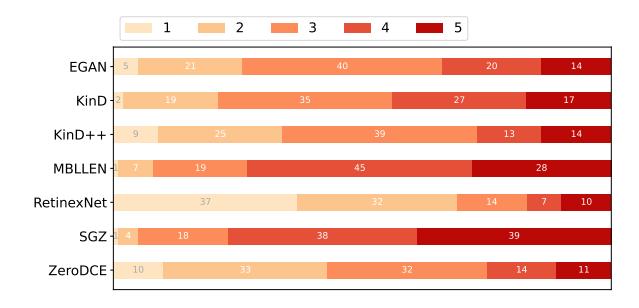


Fig. 18. Stacked bar plot from the results of the user study. Since the numbers of participants are exactly 100, the count shown in the plot is equivalent to the percentage value.

different predicted categories. Our findings are as follows 1) RetinexNet [38], MBLLEN [36], and KinD [41] causes large areas of incorrect segmentation on pedestrians and sidewalks. 2) Zero-DCE [61] and SGZ [65] are close to the GT. However, SGZ [65] results in better segmentation results for the objects in the distance.

Fig. 25 presents the qualitative comparison for a video frame from our Night Wenzhou dataset. Our findings are as below. 1) RetinexNet [38], KinD [41], and Zero-DCE [61] produces images with poor contrast, extreme color deviation, oversmoothed details, and significant noises, blurs, and artifacts. 2) EGAN [57] produces over-exposed images. 3) MBLLEN [36], KinD++ [45], and SGZ [65] produces images with good exposure. However, MBLLEN [36] oversmooths the detail, whereas KinD++ [45] generates artifacts and has more color deviation than SGZ [65].

## V. APPLICATIONS

#### A. Visual Surveillance

Visual surveillance systems have to operate 24 hours per day to capture all the essential information. However, at low-light conditions like night or dusk, it is challenging for visual surveillance systems to collect images or videos with good contrast and sufficient details [6]. This may lead to failure to catch the illegal or criminal acts, or failure to capture the party responsible for a specific accident. Over the past years, Kinect depth map [108], enhanced CNN-enabled learning [109], and SVD-DWT [110] have been used to address the visual surveillance challenges in low-light conditions.

# B. Autonomous Driving

Real-world autonomous driving often has to operate at nighttime with low-light conditions. Autonomous vehicles perform poorly at low-light conditions because their visual recognition algorithms are trained with visual data captured in good illumination conditions (e.g., sunny day). For example, an autonomous vehicle may fail to recognize (and possibly collide into) a moving pedestrian who is wearing black pants and jacket on a road without street light. Recently, DriveRetinex-Net [111], LE-Net [7], and SFNet-N [3] have been developed to improve the recognition performance for autonomous vehicles at low-light conditions.

#### C. Unmanned Aerial Vehicle

Unmanned Aerial Vehicle (UAV) is often used in aerial photography and military reconnaissance. Both tasks are usually performed in low-light conditions (e.g. dawn, dusk, or night) for better framing or concealment. For the same reason as autonomous driving, UAVs have poor performance at these low-light conditions. For instance, a UAV flying at low-light conditions may collide into a non luminous building or a tree with dark leaves. Recently, HighlightNet [112], LighterGAN [113], LLNet [35] and the IOU-predictor network [114] have been developed to improve the recognition performance for UAV at low-light conditions.

## D. Photography

Photography is often done in dawn and dusk. That's because the light at these periods are more gentle, and can help emphasize the shapes of objects. However, the low-light conditions at dawn and dusk significantly degrade the quality of mages captured at these periods. In particular, a higher ISO and a longer exposure time will not only enhance the image brightness but also introduce noise, blurs and artifacts [9]. Recent methods like MorphNet [115], RNN [116] and a learning-based auto white balancing algorithm [117] is shown helpful for photography at low-light conditions.

#### E. Remote Sensing

Remote sensing operates at all-weather, and is often used for climate change detection, urban 3D modeling, and global surface monitoring [10]. However, low-light conditions make remote sensing challenging, since the object visibility are degraded, especially from the far-distance of the remote satellite. For example, It is difficult for remote sensing satellites to accurately detect the intensity shift of human activities in regions with few artificial light sources. Methods like RICNN [5], SR [118] and RSCNN [119] can help improve the quality of remote sensing images which boost their interpretability.

# F. Microscopic Imaging

Microscopic imaging has been widely applied to automatic cell segmentation, fluorescence labeling tracking, and high-throughput experiments [11]. However, microscopic imaging is challenging at low-light conditions due to the poor visibility of micro-level details. For instance, it is difficult to identify the cell structures with the microscope under low-light conditions. VELM [120], SalienceNet [121] and CARE network [122] can be applied to improve the visibility outcomes of optical microscopy and the video documentation of organelle motion processes at low-light conditions.

## G. Underwater Imaging

Underwater imaging often occurs low-light conditions, since the lightening in deep water in very weak. This is a challenge for underwater imaging, since the visibility in these conditions is very poor, especially for the object in the far distance [12]. For example, with the existing camera technology, it is

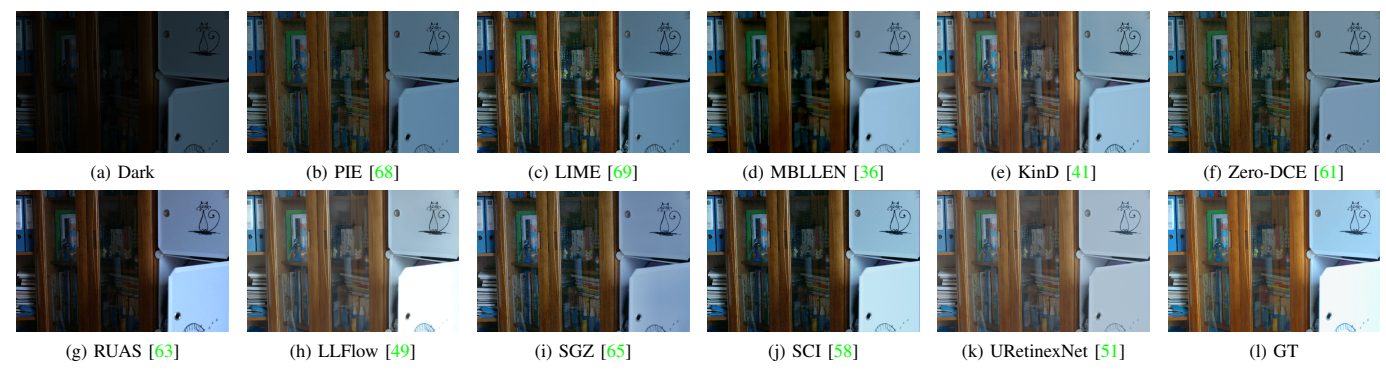


Fig. 19. Visual comparison on the LOL dataset.



Fig. 20. Visual comparison on the VV dataset.

difficult to clearly capture the details of coral reefs 30 meters below the sea level [123]. L<sup>2</sup>UWE [124], UIE-Net [125], WaterGAN [126] and UWCNN [127] have been proven useful for underwater imaging at low-light conditions.

#### VI. FUTURE PROSPECTS

#### A. Uneven Exposure

Given images or videos, existing LLIE methods correct the under-exposed region but either ignore the over-exposed region or make the over-exposed region even brighter. Real-world images and videos often exhibit uneven exposure for different regions. Ideally, the LLIE methods should brighten the under-exposed region while darkening the over-exposed region.

The future works could solve the uneven exposure challenge in the following ways. Firstly, we can collect a large-scale, real-world dataset that contains mixed over-/under-exposure in a single image. Our SICE\_Grad and SICE\_Mix is a good starting point, but more work needs to be done. Secondly, we can adopt Laplacian Pyramid (e.g., DSLR [128]) or multibranch fusion (e.g., TBEFN [129]) network to capture the multi-scale exposure information. Finally, we can leverage vision transformers [73], which can better capture global exposure information than CNNs. While IAT [56] has made the preliminary attempt in this field, its network structure could be improved to model more complex exposures.

## B. Integrating Low-Level and High-Level Tasks

The existing LLIE methods treat LLIE as a post-processing step before high-level vision algorithms. Whether this postprocessing step is beneficial to the high-level vision algorithms remains a question.

The possible next step is to integrate low-level and high-level tasks to ensure that the former contributes to the latter. Firstly, we can introduce a large-scale labeled low-light dataset for both low-level and high-level tasks. Secondly, we can perform joint training for low-level and high-level networks to benefit each other (e.g., Deblur-YOLO [130]). Finally, we can embed low-level image processing into high-level vision tasks using domain adaptation (e.g., YOLO-in-the-Dark [131]).

## C. Preserving and Utilizing Semantic Information

While enhancing the low-light regions, the existing LLIE methods may also remove the semantic information, disturbing human understanding and degrading high-level vision algorithms. Ideally, the LLIE methods should enhance the low-light regions by preserving *and* utilizing the semantic information.

The forthcoming research could attend the semantic information in the following ways. First, we could introduce a large-scale dataset with fine annotated semantic labels to ensure that the semantic information is preserved during image enhancement. In addition, we could incorporate semantic priors [132], integrate semantic-aware modules [133], or leverage semantic segmentation networks [85].

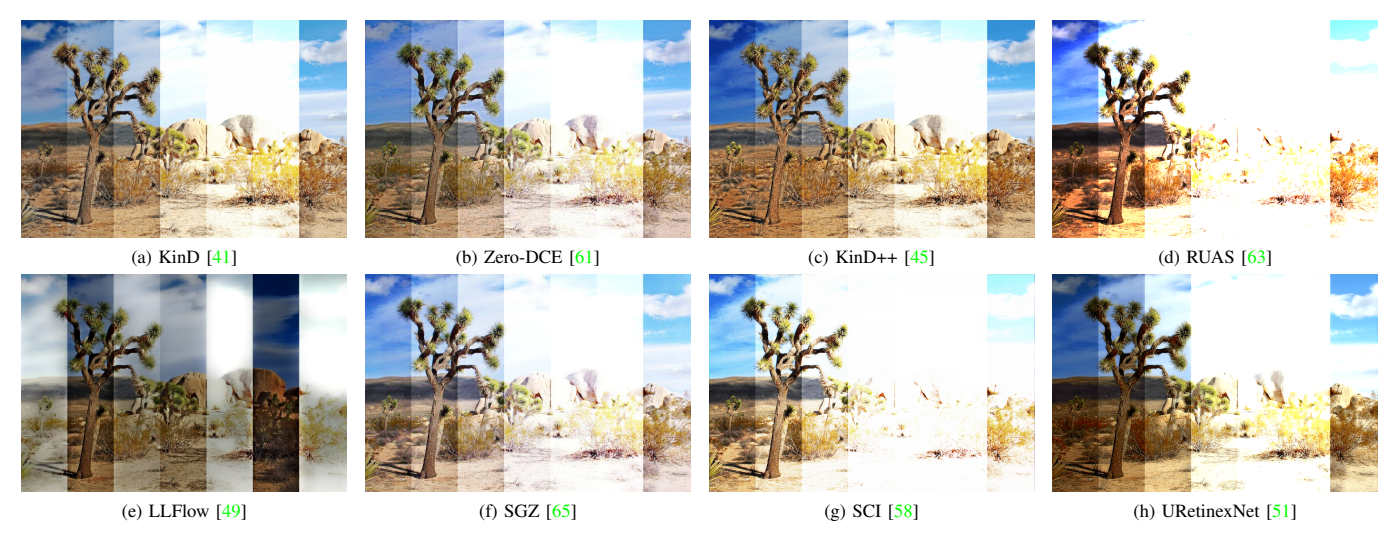


Fig. 21. Visual comparison on our SICE\_Grad dataset.

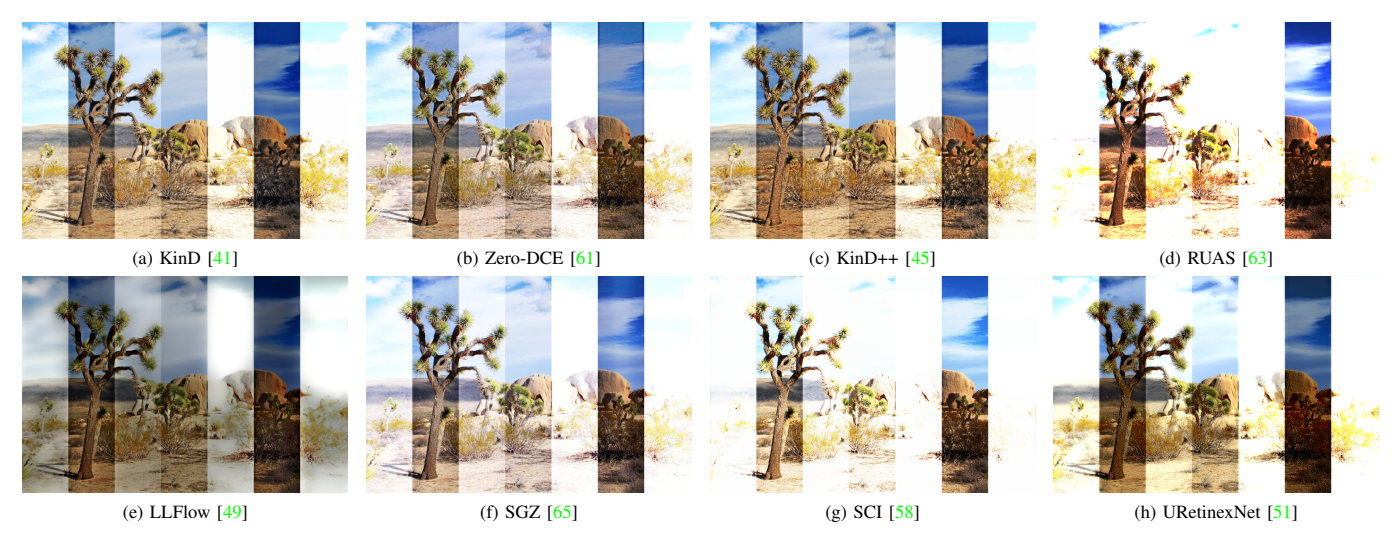


Fig. 22. Visual comparison on our SICE\_Mix dataset.

#### D. Low-Light Video Enhancement

Many existing LLIE methods cannot meet the real-time processing requirements of LLVE. Even for methods that meet the time constraint, a direct application to videos leads to flickering artifacts [1].

It is critical to improve the efficiency and effectiveness of the LLIE methods so they can generalize well to LLVE. For efficiency, we could adopt lightweight architecture using manual design (e.g., MobileNet [134]) or NAS (e.g., NasNet [135]) to improve the inference latency. For effectiveness, we could exploit temporal information from adjacent or neighbor frames to suppress flickering artifacts. Additionally, we should propose more large-scale high-resolution low-light video datasets for static and motion scenes. The introduction of Night Wenzhou is a good starting point for low-light video datasets in fast motions, but there is a long way to go.

#### E. Benchmark datasets

So far, there is no well-accepted benchmark dataset for LLIE. On the one hand, many supervised LLIE methods train

on their own dataset and generalize poorly to other datasets with significant domain gaps. On the other hand, many LLIE methods only test on their custom dataset, which is biased towards their method and unfair to others.

The subsequent works can learn from the success of CityScape [101] in semantic segmentation for benchmark training and testing. A well-accepted benchmark like CityScape includes large-scale real-world images and videos with diverse objects, has an appropriate train test split ratio, and contains ground truth annotations for high-level tasks. In LLIE, we also need to consider diverse illuminations and complex exposures.

## F. Better Evaluations Metrics

The current evaluation metrics for LLIE (e.g., PSNR and SSIM) are borrowed from other low-level vision tasks rather than designed explicitly for LLIE. In particular, methods with good scores in these evaluation metrics may not look good from the human perspective. Due to that limitation, LLIE methods heavily rely on user studies for evaluation. However,

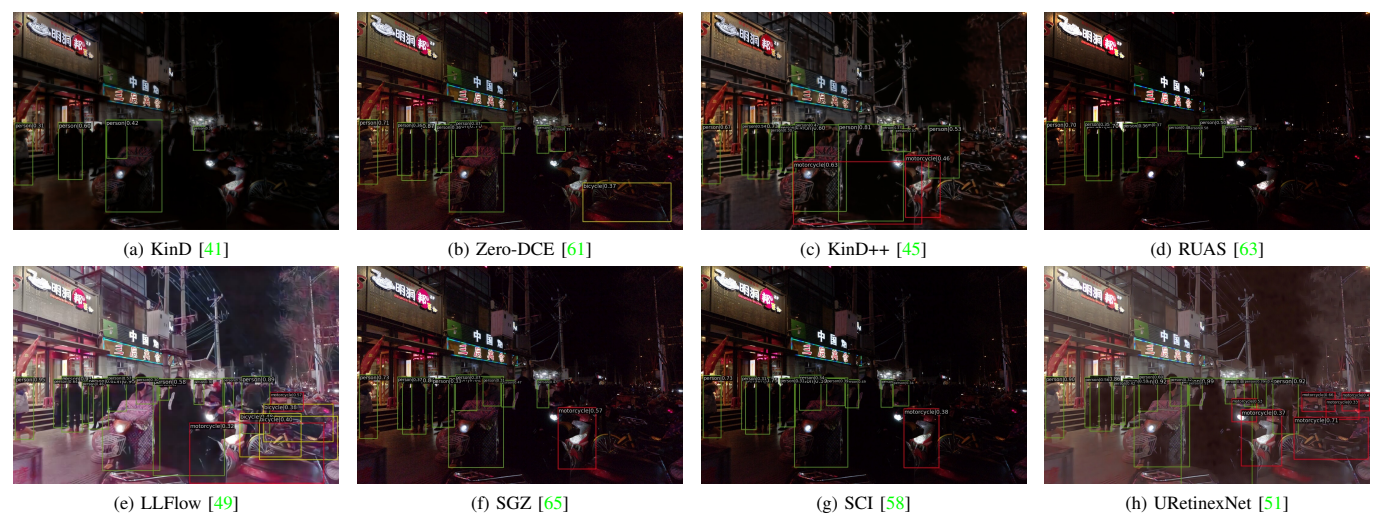


Fig. 23. Object detection comparison on DarkFace [95] dataset.

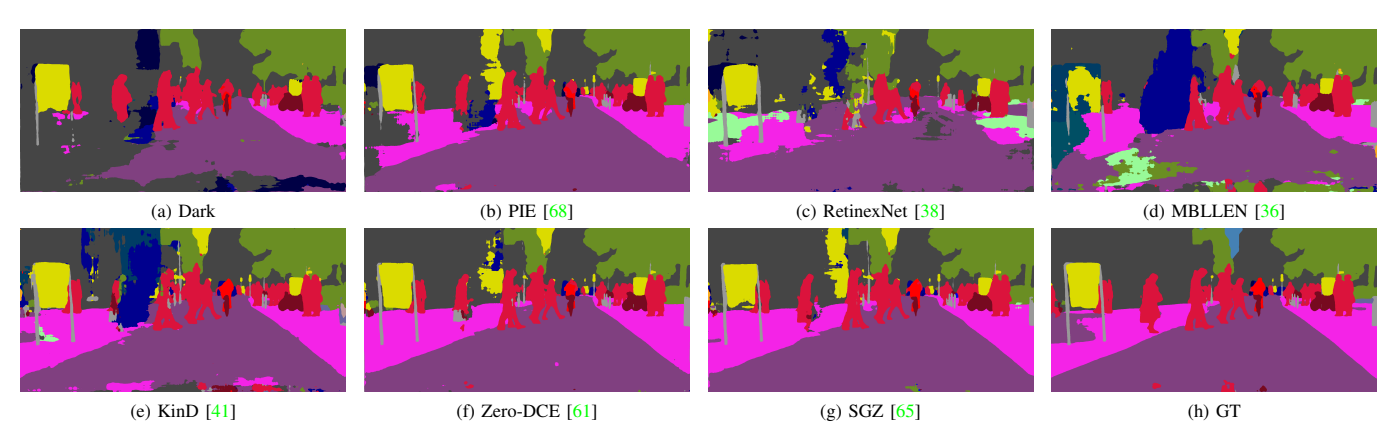


Fig. 24. Semantic segmentation comparison for the DCS [65] dataset. Note that the GT here refers to the segmentation result on the ground truth image.

a user study is expensive and time-consuming for a large-scale dataset. Therefore, A better evaluation metric is desired.

One potential direction is to propose an evaluation metric that fits the characteristic of low-light images and matches the user study scores. A recent IQA metrics MUSIQ [136] utilize an image quality transformer to attend the multi-scale multigranularity information using original-resolution images and is well-match with subjective test scores. Adapting IQA metrics like MUSIQ to the context of LLIE remains an open topic.

## G. Addressing Noises, Blurs and Artifacts

Most existing LLIE methods fail to suppress degradation like noise, blurs, and artifacts. In reality, these degradation can either exist before enhancement or appear during enhancement [137], and they deteriorate the perceptual quality of images.

The upcoming studies can solve this issue in three ways. Firstly, we can design a low-light dataset with various degradation so LLIE methods can be trained to enhance the image and tackle degradation. Secondly, we can adopt loss functions that can suppress various degradation (e.g., Adaptive TV loss [89]). Finally, we could join the task of denoising, deblurring, and LLIE in a single network (e.g., D2HNet [138]).

## H. Low-Light and Bad Weather

The present LLIE methods assume that the weather conditions are good, whereas the real-world weather is usually bad (e.g., rain, snow, haze). The combination of low-light and bad weather significantly deteriorates the visual quality, which is catastrophic for many high-level vision tasks [139].

Potentially, we can tackle the low-light and bad weather challenge in two ways. On the one hand, we can collect, synthesize, or generate low-light datasets with specific bad weather (e.g., rainy, foggy, snowy) so that LLIE methods can be trained to address bad weather and low-light conditions in one go. On the other hand, we can leverage disentangled domain adaptation to tackle LLIE in bad weather (e.g., ForkGAN [140]). It is also interesting to suppress noise and blurs within the Retinex framework (e.g., Hao et al. [141])

#### VII. CONCLUSION

This paper presents a comprehensive survey of low-light image and video enhancement. Firstly, we propose SICE\_Grad and SICE\_Mix to simulate the challenging over-/under-exposure scenes under-performed by current LLIE methods. Secondly, we introduce Night Wenzhou, a large-scale, high-resolution video dataset with various illuminations and degradation. After that, we analyze the critical components of LLIE

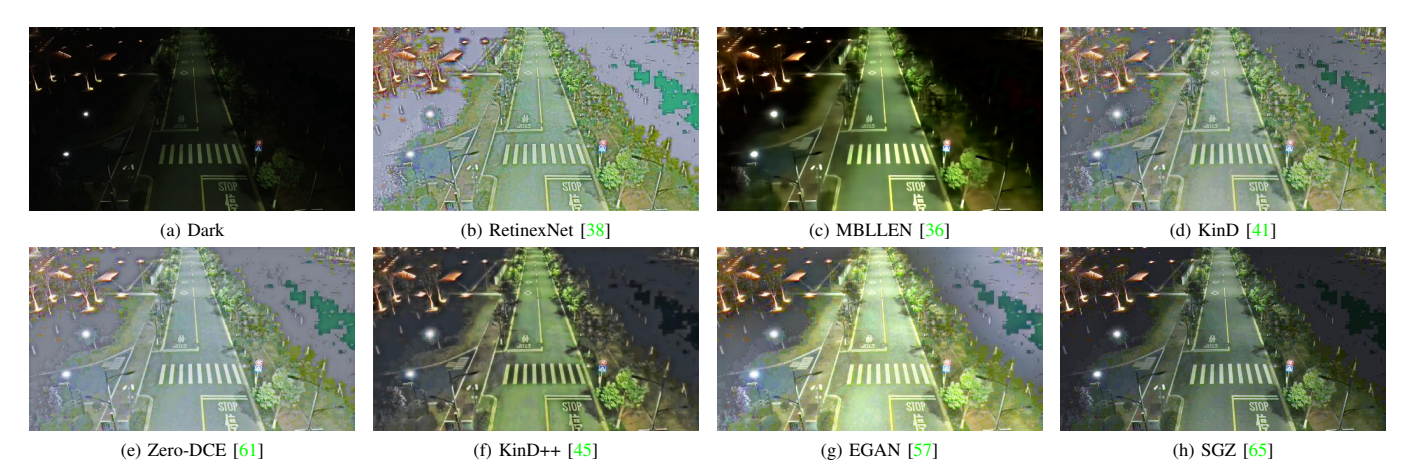


Fig. 25. Visual comparison for a video frame from our Night Wenzhou dataset.

methods, including learning strategy, network structure, loss function, evaluation metric, training and testing dataset, etc. Besides, we discuss the emerging system-level applications for low-light image and video enhancement algorithms. Finally, we conduct qualitative and quantitative comparisons of LLIE methods on the benchmark datasets and the proposed datasets to identify the open challenges and suggest future directions.

#### REFERENCES

- [1] C. Li, C. Guo, L.-H. Han, J. Jiang, M.-M. Cheng, J. Gu, and C. C. Loy, "Low-light image and video enhancement using deep learning: A survey," *IEEE transactions on pattern analysis and machine intelligence*, 2021.
- [2] Y. P. Loh and C. S. Chan, "Getting to know low-light images with the exclusively dark dataset," *Computer Vision and Image Understanding*, vol. 178, pp. 30–42, 2019.
- [3] H. Wang, Y. Chen, Y. Cai, L. Chen, Y. Li, M. A. Sotelo, and Z. Li, "Sfnet-n: An improved sfnet algorithm for semantic segmentation of low-light autonomous driving road scenes," *IEEE Transactions on Intelligent Transportation Systems*, 2022.
- [4] M. Lamba, K. K. Rachavarapu, and K. Mitra, "Harnessing multi-view perspective of light fields for low-light imaging," *IEEE Transactions* on *Image Processing*, vol. 30, pp. 1501–1513, 2020.
- [5] G. Cheng, P. Zhou, and J. Han, "Learning rotation-invariant convolutional neural networks for object detection in vhr optical remote sensing images," *IEEE Transactions on Geoscience and Remote Sensing*, vol. 54, no. 12, pp. 7405–7415, 2016.
- [6] M. Yang, X. Nie, and R. W. Liu, "Coarse-to-fine luminance estimation for low-light image enhancement in maritime video surveillance," in 2019 IEEE Intelligent Transportation Systems Conference (ITSC). IEEE, 2019, pp. 299–304.
- [7] G. Li, Y. Yang, X. Qu, D. Cao, and K. Li, "A deep learning based image enhancement approach for autonomous driving at night," *Knowledge-Based Systems*, vol. 213, p. 106617, 2021.
- [8] S. Samanta, A. Mukherjee, A. S. Ashour, N. Dey, J. M. R. Tavares, W. B. Abdessalem Karâa, R. Taiar, A. T. Azar, and A. E. Hassanien, "Log transform based optimal image enhancement using firefly algorithm for autonomous mini unmanned aerial vehicle: An application of aerial photography," *International Journal of Image and Graphics*, vol. 18, no. 04, p. 1850019, 2018.
- [9] L. Yuan, J. Sun, L. Quan, and H.-Y. Shum, "Image deblurring with blurred/noisy image pairs," in ACM SIGGRAPH 2007 papers, 2007, pp. 1–es.
- [10] J. B. Campbell and R. H. Wynne, Introduction to remote sensing. Guilford Press, 2011.
- [11] R. Pepperkok and J. Ellenberg, "High-throughput fluorescence microscopy for systems biology," *Nature reviews Molecular cell biology*, vol. 7, no. 9, pp. 690–696, 2006.
- [12] C. Li, C. Guo, W. Ren, R. Cong, J. Hou, S. Kwong, and D. Tao, "An underwater image enhancement benchmark dataset and beyond," *IEEE Transactions on Image Processing*, vol. 29, pp. 4376–4389, 2019.

- [13] S. M. Pizer, E. P. Amburn, J. D. Austin, R. Cromartie, A. Geselowitz, T. Greer, B. ter Haar Romeny, J. B. Zimmerman, and K. Zuiderveld, "Adaptive histogram equalization and its variations," *Computer vision*, graphics, and image processing, vol. 39, no. 3, pp. 355–368, 1987.
- [14] S. M. Pizer, "Contrast-limited adaptive histogram equalization: Speed and effectiveness stephen m. pizer, r. eugene johnston, james p. ericksen, bonnie c. yankaskas, keith e. muller medical image display research group," in *Proceedings of the first conference on visualization* in biomedical computing, Atlanta, Georgia, vol. 337, 1990, p. 1.
- [15] T. Arici, S. Dikbas, and Y. Altunbasak, "A histogram modification framework and its application for image contrast enhancement," *IEEE Transactions on image processing*, vol. 18, no. 9, pp. 1921–1935, 2009.
- [16] C. Lee, C. Lee, and C.-S. Kim, "Contrast enhancement based on layered difference representation of 2d histograms," *IEEE transactions* on image processing, vol. 22, no. 12, pp. 5372–5384, 2013.
- [17] K. Nakai, Y. Hoshi, and A. Taguchi, "Color image contrast enhacement method based on differential intensity/saturation gray-levels histograms," in 2013 International Symposium on Intelligent Signal Processing and Communication Systems. IEEE, 2013, pp. 445–449.
- [18] Z. Ying, G. Li, Y. Ren, R. Wang, and W. Wang, "A new low-light image enhancement algorithm using camera response model," in *Proceedings* of the IEEE international conference on computer vision workshops, 2017, pp. 3015–3022.
- [19] X. Wu, X. Liu, K. Hiramatsu, and K. Kashino, "Contrast-accumulated histogram equalization for image enhancement," in 2017 IEEE international conference on image processing (ICIP). IEEE, 2017, pp. 3190\_3194
- [20] E. H. Land and J. J. McCann, "Lightness and retinex theory," *Josa*, vol. 61, no. 1, pp. 1–11, 1971.
- [21] E. H. Land, "The retinex theory of color vision," Scientific american, vol. 237, no. 6, pp. 108–129, 1977.
- [22] C.-H. Lee, J.-L. Shih, C.-C. Lien, and C.-C. Han, "Adaptive multiscale retinex for image contrast enhancement," in 2013 International Conference on Signal-Image Technology & Internet-Based Systems. IEEE, 2013, pp. 43–50.
- [23] S. Wang, J. Zheng, H.-M. Hu, and B. Li, "Naturalness preserved enhancement algorithm for non-uniform illumination images," *IEEE transactions on image processing*, vol. 22, no. 9, pp. 3538–3548, 2013.
- [24] L. Wang, L. Xiao, H. Liu, and Z. Wei, "Variational bayesian method for retinex," *IEEE Transactions on Image Processing*, vol. 23, no. 8, pp. 3381–3396, 2014.
- [25] X. Fu, D. Zeng, Y. Huang, X.-P. Zhang, and X. Ding, "A weighted variational model for simultaneous reflectance and illumination estimation," in *Proceedings of the IEEE conference on computer vision* and pattern recognition, 2016, pp. 2782–2790.
- [26] B. Cai, X. Xu, K. Guo, K. Jia, B. Hu, and D. Tao, "A joint intrinsic-extrinsic prior model for retinex," in *Proceedings of the IEEE* international conference on computer vision, 2017, pp. 4000–4009.
- [27] X. Dong, Y. Pang, and J. Wen, "Fast efficient algorithm for enhancement of low lighting video," in ACM SIGGRAPH 2010 Posters, 2010, pp. 1–1.
- [28] L. Li, R. Wang, W. Wang, and W. Gao, "A low-light image enhancement method for both denoising and contrast enlarging," in 2015 IEEE

- international conference on image processing (ICIP). IEEE, 2015, pp. 3730–3734.
- [29] J. Y. Chiang and Y.-C. Chen, "Underwater image enhancement by wavelength compensation and dehazing," *IEEE transactions on image* processing, vol. 21, no. 4, pp. 1756–1769, 2011.
- [30] C.-Y. Li, J.-C. Guo, R.-M. Cong, Y.-W. Pang, and B. Wang, "Underwater image enhancement by dehazing with minimum information loss and histogram distribution prior," *IEEE Transactions on Image Processing*, vol. 25, no. 12, pp. 5664–5677, 2016.
- [31] T. Celik and T. Tjahjadi, "Contextual and variational contrast enhancement," *IEEE Transactions on Image Processing*, vol. 20, no. 12, pp. 3431–3441, 2011.
- [32] Z. Liang, W. Liu, and R. Yao, "Contrast enhancement by nonlinear diffusion filtering," *IEEE Transactions on Image Processing*, vol. 25, no. 2, pp. 673–686, 2015.
- [33] S.-Y. Yu and H. Zhu, "Low-illumination image enhancement algorithm based on a physical lighting model," *IEEE Transactions on Circuits and Systems for Video Technology*, vol. 29, no. 1, pp. 28–37, 2017.
- [34] H. Su and C. Jung, "Low light image enhancement based on twostep noise suppression," in 2017 IEEE International Conference on Acoustics, Speech and Signal Processing (ICASSP). IEEE, 2017, pp. 1977–1981.
- [35] K. G. Lore, A. Akintayo, and S. Sarkar, "Llnet: A deep autoencoder approach to natural low-light image enhancement," *Pattern Recognition*, vol. 61, pp. 650–662, 2017.
- [36] F. Lv, F. Lu, J. Wu, and C. Lim, "Mbllen: Low-light image/video enhancement using cnns." in *BMVC*, vol. 220, no. 1, 2018, p. 4.
- [37] C. Li, J. Guo, F. Porikli, and Y. Pang, "Lightennet: A convolutional neural network for weakly illuminated image enhancement," *Pattern* recognition letters, vol. 104, pp. 15–22, 2018.
- [38] C. Wei, W. Wang, W. Yang, and J. Liu, "Deep retinex decomposition for low-light enhancement," arXiv preprint arXiv:1808.04560, 2018.
- [39] R. Wang, Q. Zhang, C.-W. Fu, X. Shen, W.-S. Zheng, and J. Jia, "Underexposed photo enhancement using deep illumination estimation," in *Proceedings of the IEEE/CVF Conference on Computer Vision and Pattern Recognition*, 2019, pp. 6849–6857.
- [40] M. Zhu, P. Pan, W. Chen, and Y. Yang, "Eemefn: Low-light image enhancement via edge-enhanced multi-exposure fusion network," in Proceedings of the AAAI Conference on Artificial Intelligence, vol. 34, no. 07, 2020, pp. 13106–13113.
- [41] Y. Zhang, J. Zhang, and X. Guo, "Kindling the darkness: A practical low-light image enhancer," in *Proceedings of the 27th ACM interna*tional conference on multimedia, 2019, pp. 1632–1640.
- [42] K. Xu, X. Yang, B. Yin, and R. W. Lau, "Learning to restore low-light images via decomposition-and-enhancement," in *Proceedings of the IEEE/CVF Conference on Computer Vision and Pattern Recognition*, 2020, pp. 2281–2290.
- [43] L.-W. Wang, Z.-S. Liu, W.-C. Siu, and D. P. Lun, "Lightening network for low-light image enhancement," *IEEE Transactions on Image Processing*, vol. 29, pp. 7984–7996, 2020.
- [44] S. Moran, P. Marza, S. McDonagh, S. Parisot, and G. Slabaugh, "Deeplpf: Deep local parametric filters for image enhancement," in Proceedings of the IEEE/CVF conference on computer vision and pattern recognition, 2020, pp. 12826–12835.
- [45] Y. Zhang, X. Guo, J. Ma, W. Liu, and J. Zhang, "Beyond brightening low-light images," *International Journal of Computer Vision*, vol. 129, no. 4, pp. 1013–1037, 2021.
- [46] F. Zhang, Y. Li, S. You, and Y. Fu, "Learning temporal consistency for low light video enhancement from single images," in *Proceedings of the IEEE/CVF Conference on Computer Vision and Pattern Recognition*, 2021, pp. 4967–4976.
- [47] C. Zheng, D. Shi, and W. Shi, "Adaptive unfolding total variation network for low-light image enhancement," in *Proceedings of the IEEE/CVF International Conference on Computer Vision*, 2021, pp. 4439–4448.
- [48] R. Wang, X. Xu, C.-W. Fu, J. Lu, B. Yu, and J. Jia, "Seeing dynamic scene in the dark: A high-quality video dataset with mechatronic alignment," in *Proceedings of the IEEE/CVF International Conference* on Computer Vision, 2021, pp. 9700–9709.
- [49] Y. Wang, R. Wan, W. Yang, H. Li, L.-P. Chau, and A. Kot, "Low-light image enhancement with normalizing flow," in *Proceedings of the AAAI Conference on Artificial Intelligence*, vol. 36, no. 3, 2022, pp. 2604–2612.
- [50] X. Xu, R. Wang, C.-W. Fu, and J. Jia, "Snr-aware low-light image enhancement," in *Proceedings of the IEEE/CVF Conference on Computer Vision and Pattern Recognition*, 2022, pp. 17714–17724.

- [51] W. Wu, J. Weng, P. Zhang, X. Wang, W. Yang, and J. Jiang, "Uretinex-net: Retinex-based deep unfolding network for low-light image enhancement," in *Proceedings of the IEEE/CVF Conference on Computer Vision and Pattern Recognition*, 2022, pp. 5901–5910.
- [52] X. Dong, W. Xu, Z. Miao, L. Ma, C. Zhang, J. Yang, Z. Jin, A. B. J. Teoh, and J. Shen, "Abandoning the bayer-filter to see in the dark," in *Proceedings of the IEEE/CVF Conference on Computer Vision and Pattern Recognition*, 2022, pp. 17431–17440.
- [53] Z. Tu, H. Talebi, H. Zhang, F. Yang, P. Milanfar, A. Bovik, and Y. Li, "Maxim: Multi-axis mlp for image processing," in *Proceedings of the IEEE/CVF Conference on Computer Vision and Pattern Recognition*, 2022, pp. 5769–5780.
- [54] A. Dudhane, S. W. Zamir, S. Khan, F. S. Khan, and M.-H. Yang, "Burst image restoration and enhancement," in *Proceedings of the IEEE/CVF* Conference on Computer Vision and Pattern Recognition, 2022, pp. 5759–5768.
- [55] H. Wang, K. Xu, and R. W. Lau, "Local color distributions prior for image enhancement," in *European Conference on Computer Vision*. Springer, 2022, pp. 343–359.
- [56] Z. Cui, K. Li, L. Gu, S. Su, P. Gao, Z. Jiang, Y. Qiao, and T. Harada, "Illumination adaptive transformer," arXiv preprint arXiv:2205.14871, 2022.
- [57] Y. Jiang, X. Gong, D. Liu, Y. Cheng, C. Fang, X. Shen, J. Yang, P. Zhou, and Z. Wang, "Enlightengan: Deep light enhancement without paired supervision," *IEEE Transactions on Image Processing*, vol. 30, pp. 2340–2349, 2021.
- [58] L. Ma, T. Ma, R. Liu, X. Fan, and Z. Luo, "Toward fast, flexible, and robust low-light image enhancement," in *Proceedings of the IEEE/CVF* Conference on Computer Vision and Pattern Recognition, 2022, pp. 5637–5646.
- [59] W. Yang, S. Wang, Y. Fang, Y. Wang, and J. Liu, "From fidelity to perceptual quality: A semi-supervised approach for low-light image enhancement," in *Proceedings of the IEEE/CVF conference on computer* vision and pattern recognition, 2020, pp. 3063–3072.
- [60] L. Zhang, L. Zhang, X. Liu, Y. Shen, S. Zhang, and S. Zhao, "Zero-shot restoration of back-lit images using deep internal learning," in *Proceedings of the 27th ACM International Conference on Multimedia*, 2019, pp. 1623–1631.
- [61] C. Guo, C. Li, J. Guo, C. C. Loy, J. Hou, S. Kwong, and R. Cong, "Zero-reference deep curve estimation for low-light image enhancement," in *Proceedings of the IEEE/CVF Conference on Computer Vision and Pattern Recognition*, 2020, pp. 1780–1789.
- [62] C. Li, C. Guo, and C. C. Loy, "Learning to enhance low-light image via zero-reference deep curve estimation," arXiv preprint arXiv:2103.00860, 2021.
- [63] R. Liu, L. Ma, J. Zhang, X. Fan, and Z. Luo, "Retinex-inspired unrolling with cooperative prior architecture search for low-light image enhancement," in *Proceedings of the IEEE/CVF Conference on Computer Vision and Pattern Recognition*, 2021, pp. 10561–10570.
- [64] Z. Zhao, B. Xiong, L. Wang, Q. Ou, L. Yu, and F. Kuang, "Retinexdip: A unified deep framework for low-light image enhancement," *IEEE Transactions on Circuits and Systems for Video Technology*, vol. 32, no. 3, pp. 1076–1088, 2021.
- [65] S. Zheng and G. Gupta, "Semantic-guided zero-shot learning for low-light image/video enhancement," in *Proceedings of the IEEE/CVF Winter Conference on Applications of Computer Vision*, 2022, pp. 581–590.
- [66] W. Wang, X. Wu, X. Yuan, and Z. Gao, "An experiment-based review of low-light image enhancement methods," *Ieee Access*, vol. 8, pp. 87 884–87 917, 2020.
- [67] J. Liu, D. Xu, W. Yang, M. Fan, and H. Huang, "Benchmarking low-light image enhancement and beyond," *International Journal of Computer Vision*, vol. 129, no. 4, pp. 1153–1184, 2021.
- [68] X. Fu, Y. Liao, D. Zeng, Y. Huang, X.-P. Zhang, and X. Ding, "A probabilistic method for image enhancement with simultaneous illumination and reflectance estimation," *IEEE Transactions on Image Processing*, vol. 24, no. 12, pp. 4965–4977, 2015.
- [69] X. Guo, Y. Li, and H. Ling, "Lime: Low-light image enhancement via illumination map estimation," *IEEE Transactions on image processing*, vol. 26, no. 2, pp. 982–993, 2016.
- [70] H. Ibrahim and N. S. P. Kong, "Brightness preserving dynamic histogram equalization for image contrast enhancement," *IEEE Transactions on Consumer Electronics*, vol. 53, no. 4, pp. 1752–1758, 2007.
- [71] K. He, J. Sun, and X. Tang, "Single image haze removal using dark channel prior," *IEEE transactions on pattern analysis and machine* intelligence, vol. 33, no. 12, pp. 2341–2353, 2010.

- [72] O. Ronneberger, P. Fischer, and T. Brox, "U-net: Convolutional networks for biomedical image segmentation," in *International Conference on Medical image computing and computer-assisted intervention*. Springer, 2015, pp. 234–241.
- [73] A. Dosovitskiy, L. Beyer, A. Kolesnikov, D. Weissenborn, X. Zhai, T. Unterthiner, M. Dehghani, M. Minderer, G. Heigold, S. Gelly et al., "An image is worth 16x16 words: Transformers for image recognition at scale," arXiv preprint arXiv:2010.11929, 2020.
- [74] K. Zhang, L. V. Gool, and R. Timofte, "Deep unfolding network for image super-resolution," in *Proceedings of the IEEE/CVF conference* on computer vision and pattern recognition, 2020, pp. 3217–3226.
- [75] B. Zoph and Q. V. Le, "Neural architecture search with reinforcement learning," arXiv preprint arXiv:1611.01578, 2016.
- [76] D. Rezende and S. Mohamed, "Variational inference with normalizing flows," in *International conference on machine learning*. PMLR, 2015, pp. 1530–1538.
- [77] B. K. Horn and B. G. Schunck, "Determining optical flow," *Artificial intelligence*, vol. 17, no. 1-3, pp. 185–203, 1981.
- [78] D. E. Rumelhart, G. E. Hinton, and R. J. Williams, "Learning internal representations by error propagation," California Univ San Diego La Jolla Inst for Cognitive Science, Tech. Rep., 1985.
- [79] C. Goller and A. Kuchler, "Learning task-dependent distributed representations by backpropagation through structure," in *Proceedings of International Conference on Neural Networks (ICNN'96)*, vol. 1. IEEE, 1996, pp. 347–352.
- [80] C. Lu, S. Zheng, Z. Wang, O. Dib, and G. Gupta, "As-introvae: Adversarial similarity distance makes robust introvae," arXiv preprint arXiv:2206.13903, 2022.
- [81] J. Johnson, A. Alahi, and L. Fei-Fei, "Perceptual losses for realtime style transfer and super-resolution," in *European conference on computer vision*. Springer, 2016, pp. 694–711.
- [82] H. Zhao, O. Gallo, I. Frosio, and J. Kautz, "Loss functions for image restoration with neural networks," *IEEE Transactions on computational imaging*, vol. 3, no. 1, pp. 47–57, 2016.
- [83] D. Ren, W. Zuo, Q. Hu, P. Zhu, and D. Meng, "Progressive image deraining networks: A better and simpler baseline," in *Proceedings of the IEEE/CVF Conference on Computer Vision and Pattern Recognition*, 2019, pp. 3937–3946.
- [84] T. Wang, X. Yang, K. Xu, S. Chen, Q. Zhang, and R. W. Lau, "Spatial attentive single-image deraining with a high quality real rain dataset," in *Proceedings of the IEEE/CVF Conference on Computer Vision and Pattern Recognition*, 2019, pp. 12270–12279.
- [85] S. Zheng, C. Lu, Y. Wu, and G. Gupta, "Sapnet: Segmentation-aware progressive network for perceptual contrastive deraining," in Proceedings of the IEEE/CVF Winter Conference on Applications of Computer Vision, 2022, pp. 52–62.
- [86] K. Simonyan and A. Zisserman, "Very deep convolutional networks for large-scale image recognition," arXiv preprint arXiv:1409.1556, 2014.
- [87] X.-C. Liu, M.-M. Cheng, Y.-K. Lai, and P. L. Rosin, "Depth-aware neural style transfer," in *Proceedings of the Symposium on Non-Photorealistic Animation and Rendering*, 2017, pp. 1–10.
- [88] C. R. Vogel and M. E. Oman, "Iterative methods for total variation denoising," SIAM Journal on Scientific Computing, vol. 17, no. 1, pp. 227–238, 1996.
- [89] Q. Chen, P. Montesinos, Q. S. Sun, P. A. Heng et al., "Adaptive total variation denoising based on difference curvature," *Image and vision* computing, vol. 28, no. 3, pp. 298–306, 2010.
- [90] J. P. Oliveira, J. M. Bioucas-Dias, and M. A. Figueiredo, "Adaptive total variation image deblurring: a majorization-minimization approach," *Signal processing*, vol. 89, no. 9, pp. 1683–1693, 2009.
- [91] R. Zhang, P. Isola, A. A. Efros, E. Shechtman, and O. Wang, "The unreasonable effectiveness of deep features as a perceptual metric," in Proceedings of the IEEE conference on computer vision and pattern recognition, 2018, pp. 586–595.
- [92] A. Mittal, R. Soundararajan, and A. C. Bovik, "Making a "completely blind" image quality analyzer," *IEEE Signal processing letters*, vol. 20, no. 3, pp. 209–212, 2012.
- [93] K. Ma, K. Zeng, and Z. Wang, "Perceptual quality assessment for multi-exposure image fusion," *IEEE Transactions on Image Processing*, vol. 24, no. 11, pp. 3345–3356, 2015.
- [94] C. Sakaridis, D. Dai, and L. Van Gool, "Acdc: The adverse conditions dataset with correspondences for semantic driving scene understanding," in *Proceedings of the IEEE/CVF International Conference on Computer Vision*, 2021, pp. 10765–10775.
- [95] W. Yang, Y. Yuan, W. Ren, J. Liu, W. J. Scheirer, Z. Wang, T. Zhang, Q. Zhong, D. Xie, S. Pu et al., "Advancing image understanding in

- poor visibility environments: A collective benchmark study," *IEEE Transactions on Image Processing*, vol. 29, pp. 5737–5752, 2020.
- [96] V. Bychkovsky, S. Paris, E. Chan, and F. Durand, "Learning photographic global tonal adjustment with a database of input/output image pairs," in CVPR 2011. IEEE, 2011, pp. 97–104.
- [97] J. Hai, Z. Xuan, R. Yang, Y. Hao, F. Zou, F. Lin, and S. Han, "R2rnet: Low-light image enhancement via real-low to real-normal network," *Journal of Visual Communication and Image Representation*, vol. 90, p. 103712, 2023.
- [98] T. Hodan, F. Michel, E. Brachmann, W. Kehl, A. GlentBuch, D. Kraft, B. Drost, J. Vidal, S. Ihrke, X. Zabulis et al., "Bop: Benchmark for 6d object pose estimation," in Proceedings of the European conference on computer vision (ECCV), 2018, pp. 19–34.
- [99] C. Chen, Q. Chen, M. N. Do, and V. Koltun, "Seeing motion in the dark," in *Proceedings of the IEEE/CVF International Conference on Computer Vision*, 2019, pp. 3185–3194.
- [100] J. Cai, S. Gu, and L. Zhang, "Learning a deep single image contrast enhancer from multi-exposure images," *IEEE Transactions on Image Processing*, vol. 27, no. 4, pp. 2049–2062, 2018.
- [101] M. Cordts, M. Omran, S. Ramos, T. Rehfeld, M. Enzweiler, R. Benenson, U. Franke, S. Roth, and B. Schiele, "The cityscapes dataset for semantic urban scene understanding," in *Proceedings of the IEEE conference on computer vision and pattern recognition*, 2016, pp. 3213–3223.
- [102] T. S. Dee, "Teachers and the gender gaps in student achievement," Journal of Human resources, vol. 42, no. 3, pp. 528–554, 2007.
- [103] W. Zhang, K. Ma, G. Zhai, and X. Yang, "Uncertainty-aware blind image quality assessment in the laboratory and wild," *IEEE Transactions on Image Processing*, vol. 30, pp. 3474–3486, 2021.
- [104] A. Mittal, A. K. Moorthy, and A. C. Bovik, "No-reference image quality assessment in the spatial domain," *IEEE Transactions on image* processing, vol. 21, no. 12, pp. 4695–4708, 2012.
- [105] Y. Fang, H. Zhu, Y. Zeng, K. Ma, and Z. Wang, "Perceptual quality assessment of smartphone photography," in *Proceedings of the IEEE/CVF Conference on Computer Vision and Pattern Recognition*, 2020, pp. 3677–3686.
- [106] H. Zhao, J. Shi, X. Qi, X. Wang, and J. Jia, "Pyramid scene parsing network," in *Proceedings of the IEEE conference on computer vision* and pattern recognition, 2017, pp. 2881–2890.
- [107] J. Li, Y. Wang, C. Wang, Y. Tai, J. Qian, J. Yang, C. Wang, J. Li, and F. Huang, "Dsfd: dual shot face detector," in *Proceedings of the IEEE/CVF Conference on Computer Vision and Pattern Recognition*, 2019, pp. 5060–5069.
- [108] J. Hu, R. Hu, Z. Wang, Y. Gong, and M. Duan, "Kinect depth map based enhancement for low light surveillance image," in 2013 IEEE International Conference on Image Processing. IEEE, 2013, pp. 1090– 1094
- [109] R. W. Liu, W. Yuan, X. Chen, and Y. Lu, "An enhanced cnn-enabled learning method for promoting ship detection in maritime surveillance system," *Ocean Engineering*, vol. 235, p. 109435, 2021.
- [110] N. Halder, D. Roy, and A. Mitra, "Low-light video enhancement with svd-dwt algorithm for multimedia surveillance network," *Curr. Trends Signals Processing*, vol. 10, pp. 43–51, 2020.
- [111] L. H. Pham, D. N.-N. Tran, and J. W. Jeon, "Low-light image enhancement for autonomous driving systems using driveretinex-net," in 2020 IEEE International Conference on Consumer Electronics-Asia (ICCE-Asia). IEEE, 2020, pp. 1–5.
- [112] C. Fu, H. Dong, J. Ye, G. Zheng, S. Li, and J. Zhao, "Highlightnet: Highlighting low-light potential features for real-time uav tracking," arXiv preprint arXiv:2208.06818, 2022.
- [113] J. Wang, Y. Yang, Y. Chen, and Y. Han, "Lightergan: An illumination enhancement method for urban uav imagery," *Remote Sensing*, vol. 13, no. 7, p. 1371, 2021.
- [114] D. Du, P. Zhu, L. Wen, X. Bian, H. Ling, Q. Hu, J. Zheng, T. Peng, X. Wang, Y. Zhang et al., "Visdrone-sot2019: The vision meets drone single object tracking challenge results," in Proceedings of the IEEE/CVF International Conference on Computer Vision Workshops, 2019, pp. 0–0.
- [115] A. Gordon, E. Eban, O. Nachum, B. Chen, H. Wu, T.-J. Yang, and E. Choi, "Morphnet: Fast & simple resource-constrained structure learning of deep networks," in *Proceedings of the IEEE conference* on computer vision and pattern recognition, 2018, pp. 1586–1595.
- [116] W. Ren, S. Liu, L. Ma, Q. Xu, X. Xu, X. Cao, J. Du, and M.-H. Yang, "Low-light image enhancement via a deep hybrid network," *IEEE Transactions on Image Processing*, vol. 28, no. 9, pp. 4364–4375, 2019.

- [117] O. Liba, K. Murthy, Y.-T. Tsai, T. Brooks, T. Xue, N. Karnad, Q. He, J. T. Barron, D. Sharlet, R. Geiss *et al.*, "Handheld mobile photography in very low light." *ACM Trans. Graph.*, vol. 38, no. 6, pp. 164–1, 2019.
- [118] J. M. Haut, R. Fernandez-Beltran, M. E. Paoletti, J. Plaza, A. Plaza, and F. Pla, "A new deep generative network for unsupervised remote sensing single-image super-resolution," *IEEE Transactions on Geoscience* and Remote sensing, vol. 56, no. 11, pp. 6792–6810, 2018.
- [119] L. Hu, M. Qin, F. Zhang, Z. Du, and R. Liu, "Rscnn: A cnn-based method to enhance low-light remote-sensing images," *Remote Sensing*, vol. 13, no. 1, p. 62, 2020.
- [120] D. M. Shotton, "Video-enhanced light microscopy and its applications in cell biology," *Journal of Cell Science*, vol. 89, no. 2, pp. 129–150, 1988.
- [121] E. Bouilhol, E. Lefevre, T. Barry, F. Levet, A. Beghin, V. Viasnoff, X. Galindo, R. Galland, J.-B. Sibarita, and M. Nikolski, "Saliencenet: an unsupervised image-to-image translation method for nuclei saliency enhancement in microscopy images," bioRxiv, 2022.
- [122] M. Weigert, U. Schmidt, T. Boothe, A. Müller, A. Dibrov, A. Jain, B. Wilhelm, D. Schmidt, C. Broaddus, S. Culley et al., "Content-aware image restoration: pushing the limits of fluorescence microscopy," *Nature methods*, vol. 15, no. 12, pp. 1090–1097, 2018.
- [123] J. A. Goodman, S. J. Purkis, and S. R. Phinn, "Coral reef remote sensing," A guide for mapping, monitoring and management. 436p, 2013
- [124] T. P. Marques and A. B. Albu, "L2uwe: A framework for the efficient enhancement of low-light underwater images using local contrast and multi-scale fusion," in *Proceedings of the IEEE/CVF Conference on Computer Vision and Pattern Recognition Workshops*, 2020, pp. 538– 539
- [125] Y. Wang, J. Zhang, Y. Cao, and Z. Wang, "A deep cnn method for underwater image enhancement," in 2017 IEEE International Conference on Image Processing (ICIP). IEEE, 2017, pp. 1382–1386.
- [126] J. Li, K. A. Skinner, R. M. Eustice, and M. Johnson-Roberson, "Watergan: Unsupervised generative network to enable real-time color correction of monocular underwater images," *IEEE Robotics and Automation letters*, vol. 3, no. 1, pp. 387–394, 2017.
- [127] S. Anwar, C. Li, and F. Porikli, "Deep underwater image enhancement," arXiv preprint arXiv:1807.03528, 2018.
- [128] S. Lim and W. Kim, "Dslr: deep stacked laplacian restorer for low-light image enhancement," *IEEE Transactions on Multimedia*, vol. 23, pp. 4272–4284, 2020.
- [129] K. Lu and L. Zhang, "Tbefn: A two-branch exposure-fusion network for low-light image enhancement," *IEEE Transactions on Multimedia*, vol. 23, pp. 4093–4105, 2020.
- [130] S. Zheng, Y. Wu, S. Jiang, C. Lu, and G. Gupta, "Deblur-yolo: Real-time object detection with efficient blind motion deblurring," in 2021 International Joint Conference on Neural Networks (IJCNN). IEEE, 2021, pp. 1–8.
- [131] Y. Sasagawa and H. Nagahara, "Yolo in the dark-domain adaptation method for merging multiple models," in *European Conference on Computer Vision*. Springer, 2020, pp. 345–359.
- [132] W. Yang, X. Wang, A. Farhadi, A. Gupta, and R. Mottaghi, "Visual semantic navigation using scene priors," arXiv preprint arXiv:1810.06543, 2018.
- [133] S. Xie, Z. Zheng, L. Chen, and C. Chen, "Learning semantic representations for unsupervised domain adaptation," in *International conference* on machine learning. PMLR, 2018, pp. 5423–5432.
- [134] A. G. Howard, M. Zhu, B. Chen, D. Kalenichenko, W. Wang, T. Weyand, M. Andreetto, and H. Adam, "Mobilenets: Efficient convolutional neural networks for mobile vision applications," arXiv preprint arXiv:1704.04861, 2017.
- [135] B. Zoph, V. Vasudevan, J. Shlens, and Q. V. Le, "Learning transferable architectures for scalable image recognition," in *Proceedings of the IEEE conference on computer vision and pattern recognition*, 2018, pp. 8697–8710.
- [136] J. Ke, Q. Wang, Y. Wang, P. Milanfar, and F. Yang, "Musiq: Multi-scale image quality transformer," in *Proceedings of the IEEE/CVF International Conference on Computer Vision*, 2021, pp. 5148–5157.
- [137] F. Lv, Y. Li, and F. Lu, "Attention guided low-light image enhancement with a large scale low-light simulation dataset," *International Journal* of Computer Vision, vol. 129, no. 7, pp. 2175–2193, 2021.
- [138] Y. Zhao, Y. Xu, Q. Yan, D. Yang, X. Wang, and L.-M. Po, "D2hnet: Joint denoising and deblurring with hierarchical network for robust night image restoration," in *European Conference on Computer Vision*. Springer, 2022, pp. 91–110.
- [139] W. Liu, G. Ren, R. Yu, S. Guo, J. Zhu, and L. Zhang, "Image-adaptive yolo for object detection in adverse weather conditions," in *Proceedings*

- of the AAAI Conference on Artificial Intelligence, vol. 36, no. 2, 2022, pp. 1792–1800.
- [140] Z. Zheng, Y. Wu, X. Han, and J. Shi, "Forkgan: Seeing into the rainy night," in *European conference on computer vision*. Springer, 2020, pp. 155–170.
- [141] S. Hao, X. Han, Y. Guo, X. Xu, and M. Wang, "Low-light image enhancement with semi-decoupled decomposition," *IEEE transactions* on multimedia, vol. 22, no. 12, pp. 3025–3038, 2020.